UNIVERSITY OF LEEDS

Article:
Price, R, LaRowe, D, Italiano, F et al. (3 more authors) (2015) Subsurface hydrothermal processes and the bioenergetics of chemolithoautotrophy at the shallow-sea vents off Panarea Island (Italy). Chemical Geology, 407. 21 - 45. ISSN 0009-2541

https://doi.org/10.1016/j.chemgeo.2015.04.011

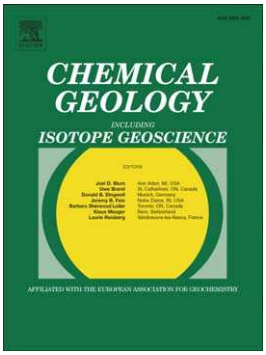

Subsurface hydrothermal processes and the bioenergetics of chemolithoautotrophy at the shallow-sea vents off Panarea Island (Italy)

Roy E. Price, Douglas E. LaRowe, Francesco Italiano, Ivan Savov, Thomas Pichler, Jan P. Amend

PII: S0009-2541(15)00199-0
DOI: doi: 10.1016/j.chemgeo.2015.04.011
Reference: CHEMGE 17560

To appear in: *Chemical Geology*

Received date: 3 September 2014
Revised date: 14 April 2015
Accepted date: 18 April 2015

Please cite this article as: Price, Roy E., LaRowe, Douglas E., Italiano, Francesco, Savov, Ivan, Pichler, Thomas, Amend, Jan P., Subsurface hydrothermal processes and the bioenergetics of chemolithoautotrophy at the shallow-sea vents off Panarea Island (Italy), *Chemical Geology* (2015), doi: 10.1016/j.chemgeo.2015.04.011

Subsurface hydrothermal processes and the bioenergetics of chemolithoautotrophy at the shallow-sea vents off Panarea Island (Italy)

Authors

Roy E. Price[a,b*], Douglas E. LaRowe[a], Francesco Italiano[c], Ivan Savov[d], Thomas Pichler[e] and Jan P. Amend[a,f]

[a] Dept. of Earth Sciences, University of Southern California, Los Angeles, CA, USA

[b] current address: SUNY Stony Brook, School of Marine and Atmospheric Sciences, Stony Brook, NY, USA

[c] National Institute of Geophysics and Volcanology (INGV), Palermo, Italy

[d] School of Earth and Environment, University of Leeds, Leeds, United Kingdom

[e] Geochemistry Department, University of Bremen, Germany

[f] Dept. of Biological Sciences, University of Southern California, Los Angeles, California, USA

* **corresponding:** E-mail: **Roy.Price@stonybrook.edu.** Ph: 631.632.8700. Fx: 631.632.8820

Abstract

The subsurface evolution of shallow-sea hydrothermal fluids is a function of many factors including fluid-mineral equilibria, phase separation, magmatic inputs, and mineral precipitation, all of which influence discharging fluid chemistry and consequently associated seafloor microbial communities. Shallow-sea vent systems, however, are understudied in this regard. In order to investigate subsurface processes in a shallow-sea hydrothermal vent, and determine how these physical and chemical parameters influence the metabolic potential of the microbial communities, three shallow-sea hydrothermal vents associated with Panarea Island (Italy) were characterized. Vent fluids, pore fluids and gases at the three sites were sampled and analyzed for major and minor elements, redox-sensitive compounds, free gas compositions, and strontium isotopes. The corresponding data were used to 1) describe the subsurface geochemical evolution of the fluids and 2) to evaluate the catabolic potential of 61 inorganic redox reactions for in situ microbial communities. Generally, the vent fluids can be hot (up to 135 °C), acidic (pH 1.9-5.7), and sulfidic (up to 2.5 mM H_2S). Three distinct types of hydrothermal fluids were identified, each with higher temperatures and lower pH, Mg^{2+} and SO_4^{2-}, relative to seawater. Type 1 was consistently more saline than Type 2, and both were more saline than seawater. Type 3 fluids were similar to or slightly depleted in most major ions relative to seawater. End-member calculations of conservative elements indicate that Type 1 and Type 2 fluids are derived from two different sources, most likely 1) a deeper, higher salinity reservoir and 2) a shallower, lower salinity reservoir, respectively, in a layered hydrothermal system. The deeper reservoir records some of the highest end-member Cl concentrations to date, and developed as a result of recirculation

of brine fluids with long term loss of steam and volatiles due to past phase separation. No strong evidence for ongoing phase separation is observed. Type 3 fluids are suggested to be mostly influenced by degassing of volatiles and subsequently dissolution of CO_2, H_2S, and other gases into the aqueous phase. Gibbs energies (ΔG_r) of redox reactions that couple potential terminal electron acceptors (O_2, NO_3^-, Mn^{IV}, Fe^{III}, SO_4^{2-}, S^0, CO_2,) with potential electron donors (H_2, NH_4^+, Fe^{2+}, Mn^{2+}, H_2S, CH_4) were evaluated at in situ temperatures and compositions for each site and by fluid type. When Gibbs energies of reaction are normalized per kilogram of hydrothermal fluid, sulfur oxidation reactions are the most exergonic, while the oxidation of Fe^{2+}, NH_4^+, CH_4, and Mn^{2+} are moderately energy yielding. The energetics calculations indicate that the most robust microbial communities in the Panarea hot springs combine H_2S from deep water-rock-gas interactions with O_2 that is entrained via seawater mixing to fuel their activities, regardless of site location or fluid type.

Key Words: Shallow-sea, hydrothermal, subsurface processes, bioenergetics, microbial metabolism, thermodynamics, biogeochemistry

1. Introduction

Marine hydrothermal vent fluids are often highly enriched in reducing inorganic chemical species (electron donors) which, when mixed with oxidized seawater, can generate aqueous solutions with multiple redox disequilibria. In deep-sea vent environments, microbial communities take advantage of these energy sources and comprise the base of the food web for some of the most diverse ecosystems on the planet (Felbeck and Somero, 1982; Imhoff and Hügler, 2009; Lutz and Kennish, 1993). However, these hydrothermal mixing regimes are not limited to the deep sea. Shallow-sea vent fluids also mix with seawater to establish redox gradients (Akerman et al., 2011; Amend et al., 2003a; Dando et al., 1999; Fitzsimons et al., 1997; Meyer-Dombard et al., 2011; Price and Pichler, 2005). Shallow-sea hydrothermal vents are generally defined as occurring at a water depth < 200 m, a depth which marks the deepest extent of the photic zone and coincides with a large change in the slope of the seawater boiling curve (Tarasov et al., 2005). They are often accompanied by abundant free gas discharges. As a result, shallow-sea hydrothermal systems are often referred to as 'gasohydrothermal' vents, and have been documented on the summits of seamounts, on the flanks of volcanic islands, and in other near-shore environments characterized by high heat flow (Italiano and Nuccio, 1991; Pichler, 2005; Price et al., 2013a; Tarasov et al., 2005). Their easy accessibility, relative to deep-sea hydrothermal systems, makes them excellent natural laboratories to study a wide range of chemical, physical, and biological processes (Pichler et al., 2006).

The subsurface geochemical processes controlling the composition of discharging hydrothermal fluids at deep-sea vents are manifold, and have been investigated and

reviewed extensively (e.g., see Alt, 1995; Berndt et al., 1988; Bischoff and Rosenbauer, 1985; Fournier, 2007; Foustoukos and Seyfried, 2007; German and Von Damm, 2003; Hannington et al., 2005; Hedenquist and Lowenstern, 1994; Heinrich et al., 2004; Henley and Ellis, 1983; Seyfried and Mottl, 1982; Tivey, 2007). The final compositions are a function of many factors including fluid-mineral equilibrium, phase separation, magmatic inputs, mineral precipitation, and mixing. While these processes have been well defined for deep-sea systems along mid-ocean ridges, and more recently at back-arc basins (Reeves et al., 2011), much less is known about the subsurface processes taking place at shallow-sea hydrothermal vents. They are most often associated with island arc volcanoes, and thus silicic magmas more similar to back-arc basins rather than mid-ocean ridges. Shallow-sea vents occur within the photic zone, and can have meteorically derived groundwater as a potential source fluid. These characteristics, combined with their occurrence in lower pressure environments, begs the question of what consequences this has for the evolution of fluid chemistry and how this in turn influences the related seafloor microbial communities.

The quest for energy is a key function of all living systems (Schroedinger, 1944), and the potential metabolic activities of microorganisms in shallow-sea hydrothermal systems can be determined by calculating the Gibbs energy of reactions between the electron donors and acceptors present in discharging fluids. This type of thermodynamic analysis of potential microbial metabolisms has been successfully conducted in many environments, including several submarine (Amend et al., 2011; Amend and Shock, 2001; Hernandez-Sanchez et al., 2014; LaRowe and Amend, 2014; LaRowe et al., 2008; McCollom, 2000; McCollom, 2007; McCollom and Shock, 1997; Shock and Holland,

2004; Shock et al., 1995; Teske et al., 2014), and terrestrial hydrothermal systems (Inskeep et al., 2005; Inskeep and McDermott, 2005; Shock et al., 2010; Spear et al., 2005; Vick et al., 2010; Windman, 2010). Unfortunately, energetic profiles of shallow-sea hydrothermal systems are rare, despite the fact that their diverse geochemistry accounts for a large number of potential catabolic strategies.

In this communication, geochemical data are presented for vent and pore fluids collected from 2008 to 2010 from three distinct sites in the shallow-sea hydrothermal system off Panarea Island (Italy). The main purpose of this paper is to describe the variability of vent fluid chemistry between sites, and understand how this variability evolved as a result of subsurface hydrothermal processes. As a secondary but logical extension of this analysis, geochemical data are then used to calculate in situ redox reaction energetics in order to link subsurface geochemical processes and the resulting differences in vent chemistry, as understood through our geochemical data, to potential microbial metabolisms.

2. Site Characteristics

2.1. Bedrock Lithology

Panarea Island is part of the Aeolian arc, a string of islands and several seamounts just north of Sicily (Italiano & Nuccio, 1991; Fig. 1a and 1b). Panarea and the associated islets were emplaced on ~15–20 km thick continental crust (Neri et al., 2002), and are located between the active volcanoes of Vulcano and Lipari in the southwest and Stromboli in the northwest part of the arc (Fig. 1a). Several investigations have suggested that the western and eastern islands along the arc are structurally and compositionally

distinct (Calanchi et al., 2002; De Astis et al., 2000; Peccerillo, 2001; Peccerillo and Panza, 1999). Rocks from the western arc are calc-alkaline and have compositions that suggest a genesis within a MORB-type mantle with modification by fluids and melts released from an oceanic slab (Ellam et al., 1989; Francalanci et al., 1993). However, to the east, Stromboli shows calc-alkaline to potassic-alkaline rocks with lower large ion lithophile element (LILE)/high field strength element (HFSE) ratios along with more radiogenic isotopic Sr composition than rocks from the western arc (Calanchi et al., 2002; De Astis et al., 2000; Ellam et al., 1989). Thus, the source rocks beneath Panarea are a mixture of these two sources, i.e., partially western arc mantle and partially Stromboli mantle (Calanchi et al., 2002), and hydrothermal fluids could be reacting with either or both of these bedrock lithologies.

2.2. Hydrothermal Activity and Sampling

Free gas bubbles and aqueous fluids vent at ~20 m below sea level depth near La Calcara beach (~50 to 200 m offshore; Fig. 1b). More intense hydrothermal activity with focused and diffuse venting occurs at several sites ~2 km offshore in 18 to 25 m water depth, inside a submerged caldera (Fig. 1b). In both areas, emissions are marked by white deposits of colloidal sulfur associated with microbial activity (Gugliandolo et al., 1999; Italiano and Nuccio, 1991; Maugeri et al., 2009).

Sampling efforts in this study focused on three distinct sites near Panarea Island: Hot Lake, Black Point, and La Calcara (see Fig. 1b). Hot Lake, located in the main submerged caldera (Latitude 38°38'19.3032", Longitude 15°06'32.7511"), is an oval-shaped (~ 4 by 6 m), ~2.5 m deep depression in the seafloor partially filled with thick

white mats of elemental sulfur and associated microorganisms (Fig. 2a). Diffuse venting of a warm (up to 80 °C) hydrothermal brine appears to fill the small depression from below, but very little free gas (i.e., as venting gas bubbles) is visible. Black Point, also located within the main caldera (Latitude 38°38'13.9961", Longitude 15°06'18.0177"), is a large (~20 by 25 m) sediment-filled basin with vigorous gas and fluid venting (Fig. 2b), and is named for a ~0.5 m tall smoker-type chimney located within the basin (noted in Fig. 2b). The vent fluids and outer-most mineralized zone of the chimney are enriched in Fe and Mn, consisting of metal sulfides and oxides, including galena, pyrite, marcasite, sphalerite, as well as the barium sulfate mineral barite (Becke et al., 2009). The La Calcara site is an expansive area of sediments several hundred square meters in size characterized by diffuse hydrothermal gas and water venting, located outside the main caldera and just offshore Panarea (Fig. 2c; Latitude 38°38'40.7129", Longitude 15°04'32.6926"). Sediment ripples are commonly crested with white mats; orange-red sediments (presumably Fe- and Mn-oxides) occur along the periphery. In some areas at La Calcara, gas venting is very intense, similar to that occurring at Black Point, but fluid flow rates never approach what would be considered a typical "focused" hydrothermal vent (Fig. 2c). Fluids collected from one of these intense gas venting areas at La Calcara are referred to as "gas-rich fluids" (GRF) for the remainder of the manuscript.

3. Methods

3.1 Sampling and geochemical analyses

Three types of fluids were collected by SCUBA divers: 1) focused vent fluids, VF (only at Black Point), 2) fluids associated with free gas emissions (only at La Calcara;

GRF = gas-rich fluids), and 3) pore fluids (from all 3 sites; SPF and RPF, see below). VF and GRF were both collected with BD® sterile 60 mL syringes from the outlet of an inverted funnel placed over the vent after the temperatures of the exiting fluids stabilized. Pore fluids were collected in 2 different ways: syringe pore fluids (SPF) were collected from ~10 cm sediment depth by inserting a small (~1 cm diameter) polycarbonate tube with a pipette tip attached, and slowly drawing fluids into BD® sterile 60 mL syringes. To minimize seawater contamination, the first 20 ml of each sample were discarded through a 3-way valve. Rhizon pore fluids (RPF) were obtained from sediment cores collected with polycarbonate tubes and rubber end caps (Seeberg-Elverfeldt et al., 2005). Background seawater was sampled ~1 km from the area of hydrothermal venting.

Temperatures were measured in situ with probes in a custom-built underwater housing (Max Planck Institute for Marine Microbiology, Bremen, Germany). Onshore, a WTW pH meter 3210 and a Mic-D electrode with temperature compensation was used to measure the pH of each sample. Aliquots for H_2S concentration measurements were preserved in the field by the addition of 1 ml of a 50 mM zinc acetate solution to 3 ml of sample to precipitate zinc sulfide. The preserved sample aliquots were then frozen. Once back in the laboratory, aliquots were thawed and analyzed for decreased light intensity caused by the ZnS precipitate with a Merck photometer at a wavelength of 670 nm (Cline, 1969; Moest, 1975). Alkalinity titrations were performed following the methods of Grasshoff et al. (1983). Analytical uncertainties were approximately ± 0.1 ºC for temperature, ± 0.1 for pH, and ± 5 % for H_2S and alkalinity measurements.

Samples for anion (Br, Cl, SO_4) analyses were filtered in the field (using a 0.2 μm mesh) and then frozen until measurement by ion chromatography (Dionex IC system

housed at the University of Bremen). No salt precipitation was observed after thawing. Samples for elemental analyses (Na, Ca, K, B, Sr, Si, Ba, Mn, and Fe) were filtered in the field (0.2 μm) and acidified using ultrapure double distilled HNO_3 to 1 % by volume (note: for all vent samples, Si exists as H_4SiO_4 (Gunnarsson and Arnorsson, 2000), but will be referred to as Si for the remainder of this paper). The preserved sample elemental concentrations were then measured by inductively coupled plasma – optical emission spectrometry (Perkin-Elmer Optima 3300 ICP-OES housed at the University of Bremen). Li, Rb, and Cs were measured by high-resolution double-focusing inductively coupled plasma – mass spectrometry (Thermo Finnigan Element 2 ICP-MS housed at the University of Bremen). The instrument limit of detection (LOD; in □g/L unless otherwise noted) for each element analyzed, calculated by multiplying 3 by the standard deviation of a blank sample, was: Na (3), Ca (0.01), K (0.27), B (0.05), Sr (0.19 μg/L), Si (0.42 μg/L), Ba (0.21 μg/L), Mn (0.32 μg/L), Fe (2.4 μg/L), Li (20.7 ng/L), Rb (10.0 ng/L), Cs (4.6 ng/L), Cl (0.2), Br (0.1), and SO_4 (0.2). The analytical uncertainty, determined by averaging the uncertainties of field duplicates, was consistently better than 2 % for Na, Ca, K, B, Sr, Si, Ba, and Mn, and better than 3% for Fe. Chloride, Br, and SO_4 uncertainties were consistently better than 0.5%, while uncertainties for Li, Rb, and Cs were consistently better than 3, 2, and 1 %, respectively. Dilution was necessary in order to account for the high salt content in the fluid samples, and all data are blank and dilution corrected.

Gas sampling was carried out by first placing a stainless steel funnel, with the large opening in the sediments, over an area of gas bubble venting (Müller, 2011). Glass sampling tubes with valves on each end were filled with seawater before the dive, then

connected to the top of the funnel. Once the gas had completely replaced the seawater and flushed through for approximately 1 minute, the valves were closed. Samples were then transferred to the National Institute of Geophysics and Volcanology (INGV) for analysis. The dissolved gases were extracted from water samples after the attainment of equilibrium (at constant temperature) between the water sample and a known volume of high purity argon, which was injected inside the sampling bottle (Müller, 2011). Analyses were carried out by a Perkin Elmer 8500 gas chromatograph equipped with a double-detector (TCD-FID) using argon as carrier gas.

Samples for Sr isotope analysis were selected across the range of temperature and Mg concentrations, and prepared following the method described in Price et al. (2013b). Briefly, sample splits (0.2 to 1 mL) were transferred into 15 mL Teflon beakers and dried down on a hotplate at <80 °C. The solid, pure white residue was then dissolved in a 4 ml mixture of ultrapure double distilled concentrated HF and HNO_3 (proportion of 3:1 by volume). The sealed Teflon beakers were left on a hotplate for 48 h at ~90 °C to ensure complete digestion. The samples were dried and subsequently re-dissolved first in ultrapure concentrated HNO_3 and then in ultrapure concentrated HCl acid. Finally, the dried solid residues were re-dissolved in 2.5 M ultrapure HCl, centrifuged, and passed through a cation exchange column to purify the Sr. The same procedure is used for routine rock analysis and ensures that all mineral phases are effectively dissolved, which provides a high degree of confidence that our analyses are representative of the entire sample. The purified Sr splits (14 ml) were dried on a hotplate, re-dissolved in 2 M HCl and then ~1/6 to ~1/8 of the sample was loaded onto outgassed W filaments coated in a $TaCl_5$ solution.

Strontium isotope ratios were measured on a Thermo Scientific TRITON-series multi-collector thermal ionization mass spectrometer (MC-TIMS, Univ. Leeds) running in static mode. The $^{87}Sr/^{86}Sr$ ratios were normalized to an $^{86}Sr/^{88}Sr$ ratio of 0.1194 to account for mass fractionation. The reported $^{87}Sr/^{86}Sr$ values were normalized to NIST SRM-987 standard values of $^{87}Sr/^{86}Sr = 0.710248$ (McArthur et al., 2000). The instrumental errors were always better than 6×10^{-6} of the mean of 180 single determinations. The total blank concentrations for Sr were negligible (<100 pg) compared to the Sr concentration of the samples analyzed.

The saturation index of anhydrite, $\Omega_{anhydrite}$, was calculated as a function of temperature using

$$\Omega_{anhydrite} = IAP/K_{sp} \quad (1)$$

where IAP and K_{sp} stand for the ion activity product and saturation product of anhydrite, respectively. Values of IAP are calculated using

$$IAP = a_{Ca^{2+}} \cdot a_{SO_4^{2-}} \quad (2)$$

and the activities of Ca^{2+} and SO_4^{2-}, $a_{Ca^{2+}}$ and $a_{SO_4^{2-}}$, respectively, are calculated using the concentrations of these species in seawater, 11 mm and 28 mm, and

$$a_i = \gamma_i \left(\frac{C_i}{C_i^{\theta}} \right) \quad (3)$$

γ_i stands for the activity coefficient of the ith species and C_i and C_i^{θ} denote the concentrations of the ith species in seawater and under standard state conditions, respectively. Standard state conditions for aqueous species stipulate that the concentrations of a species is taken to be equal to one molal referenced to infinite dilution. Values of $\square_i$ were in turn computed as a function of temperature and ionic strength using an extended version of the Debye-Hückel equation (Helgeson, 1969). Values of K_{sp} were calculated as a function of temperature and pressure in the same manner as the other equilibrium constants (see below).

End-member concentrations were calculated using the 'zero-Mg' method, which assumes all magnesium has been removed from the hydrothermal reservoir fluids prior to any mixing with seawater. In this case, the end-member compositions were calculated according to the following formula:

$$X_{hf} = \frac{Xm - Xsw\ (Mgm/Mgsw)}{1-\ (Mgm/Mgsw)} \qquad (4)$$

where X_{hf} is the calculated end-member concentration, X_m is the measured concentration and X_{sw} is the concentration in seawater (Pichler et al., 1999).

3.2 Bioenergetic computations

The amount of Gibbs energy available from a given chemical reaction (ΔG_r) can be calculated using

$$G_r = RT \ln \frac{K_r}{Q_r}, \quad (5)$$

where K_r and Q_r refer to the equilibrium constant and reaction quotient of the reaction, respectively, R represents the gas constant, and T denotes temperature in Kelvin. ΔG_r is then divided by the number of electrons in each metabolic reaction to give moles per electron transferred. Values of K_r were calculated using the revised-HKF equations of state (Helgeson et al., 1981; Shock et al., 1992; Tanger and Helgeson, 1988), the SUPCRT92 software package (Johnson et al., 1992), and thermodynamic data taken from (Schulte et al., 2001; Shock and Helgeson, 1988; Shock and Helgeson, 1990; Shock et al., 1989; Sverjensky et al., 1997). Values of Q_r were calculated using

$$Q_r = \prod_i a_i^{\nu_i}, \quad (6)$$

where a_i stands for the activity of the ith species and ν_i corresponds to the stoichiometric coefficient of the ith species in the reaction of interest. Molalities of the ith species, m_i, were converted into activities using individual activity coefficients of the ith species (γ_i),

$$a_i = m_i \gamma_i . \quad (7)$$

Values of γ_i were in turn computed as a function of temperature and ionic strength using an extended version of the Debye-Hückel equation (Helgeson, 1969).

Values were also normalized to energy per kg of H_2O, E_{H_2O}, and were calculated using (LaRowe and Amend, 2014):

$$E_{H_2O} = \frac{-\Delta G_r}{v_i} * [i] \quad (8)$$

where ΔG_r refers to the Gibbs energy of reaction per reaction turnover, v_i stands for the stoichiometric coefficient of the ith species and [i] represents the molal concentration of the ith electron donor or acceptor per kg of seawater.

4. Results

Field and laboratory geochemical data for three hydrothermal sites at Panarea are presented in Table 1. Data are arranged by site (Hot Lake, Black Point, and La Calcara), then by sample type (RPF, SPF, VF or GRF) within each site grouping, and finally with RPF fluids arranged subsequently by depth. In situ pore fluid temperatures were generally 35 to 80 °C at Hot Lake, 40-100 °C at Black Point, and 45-80 °C at La Calcara (Figs. 3a and 3b). The zone with the most vigorous gas venting measured up to 135 °C at ~10 cm into the sediments at La Calcara. Vent fluids at Black Point also reached 134 °C, which is consistent with more than 2 decades of measurements from these sites (Italiano & Nuccio, 1991). The pH of pore fluid at the three sites was commonly circumneutral to slightly acidic (5-7), with a few measurements at Hot Lake and Black point more acidic (~3; Table 1; Figs. 3a and 3c). Pore fluid H_2S concentrations were higher at Hot Lake (up to 2.5 mM) than at Black Point (up to 0.61 mM) and La Calcara (consistently

indistinguishable from the detection limit (0.01 mM); Figs. 3b and 3c). For comparison, ambient seawater temperature was ~20 °C, pH 8.0, and H_2S concentrations were below detection.

Overall, major element concentrations (that is, the elements typically found in highest concentrations in seawater) were highly variable. Magnesium concentrations ranged from 35 to 60.4 mM in the vent fluids, while seawater was 58.3 mM (note: salinity of Mediterranean seawater is generally higher (~38‰) than 'typical' seawater (~35‰) as a result of evaporation without sufficient rainfall to balance outputs). Sulfate concentrations in vent fluids ranged from 5.4 to 32.1 mM, less than the seawater concentration of 32.9 mM. On a site-by-site comparison, Hot Lake fluids are generally more depleted in Mg and SO_4, and more enriched in all of the other major and trace elements, compared to the other two sites (Table 1). The other major cations, Na, Ca, K, B, and Sr had mM concentrations ranging from 452 to 740, 9.1 to 390.0, 8.5 to 86.7, 0.3 to 20.2, and 0.08 to 2.0, respectively. This is compared to seawater values of 547, 11.1, 11.0, 0.46, and 0.09 mM, respectively. Bromine and Cl ranged from 0.3 to 2.2 and 510 to 1410 mM, which compared to seawater values of 0.94 and 618 mM, respectively.

Trace element concentrations were highly variable. Like the major elements (except Mg and SO_4), they typically showed enrichment over seawater values. Silica ranged from 0.01 to 3.5 mM, with seawater concentration of 0.04. Iron, Mn, Ba, Li and Rb were all in the μM range, with concentrations ranging from below detection to 354, 0.1 to 9050, 0.1 to 21.5, 8.3 to 6180, and 1.0 to 275, respectively. Seawater concentrations of Fe and Mn were below detection by our analysis method, and we have reported published values of 0.017 μM (Achterberg et al., 2001) and 0.0055 μM (Lan and

Alfassi, 1994), respectively. Cesium concentrations showed orders of magnitude variability, ranging from the seawater value of 2.0 to as high as 47090 nM.

Strontium isotopic ratios for selected samples ranged 0.709208 to 0.706642. Seawater $^{87}Sr/^{86}Sr$ was 0.709160. Although sparse, the $^{87}Sr/^{86}Sr$ data seem to reflect the special character of Hot Lake fluids, having the least radiogenic value (0.706642).

5.0 Discussion

The location in a hydrothermal system where hydrothermal processes take place can be divided into three main areas - the recharge, subseafloor reaction, and discharge zones - which in reality cover a continuum of processes occurring in a dynamic system (Alt, 1995). In a simplified model, the major processes affecting hydrothermal vent fluid chemistry take place as follows: Heating up of the cold, entrained seawater which has entered the crust in the recharge zone, and the onset of low temperature water-rock reactions (Berndt and Seyfried, 1993; Berndt et al., 1988). This includes oxidation/alteration of the crust, and fixation of Mg, alkalis and B (Alt, 1995). This process forms smectite at lower temperatures and chlorite at higher temperatures, and can be generally described by the following reaction (Tivey, 2007):

$$4(NaSi)_{0.5}(CaAl)_{0.5}AlSi_2O_8 + 15Mg^{2+} + 24H_2O \Rightarrow$$

$$3Mg_5Al_2Si_3O_{10}(OH)_8 + SiO_2 + 2Na^+ + 2Ca^{2+} + 24H^+ \qquad (9)$$

where $4(NaSi)_{0.5}(CaAl)_{0.5}AlSi_2O_8$ represents anorthite+albite making up the basement rocks, and $3Mg_5Al_2Si_3O_{10}(OH)_8$ is chlorite. Note that abundant Na and Ca is mobilized,

along with SiO_2 and concomitant acidification. However, experimental results suggest that uptake of Mg by rock is more or less balanced by mobilization of Ca to the fluids (Bischoff and Rosenbauer, 1989; Mottl, 1983). Most of this Ca will combine with SO_4 and be removed by subsequent precipitation of anhydrite ($CaSO_4$; Alt, 1995). Continued heating in the "subsurface reaction zone" of the hydrothermal system causes high temperature reactions that include mobilization of alkalis, Fe and Mn (Alt, 1995; Alt et al., 1986; German and Von Damm, 2003). Deeper in the system, anorthite is altered to albite, a process called albitization, with Na and Si being added to the crust in exchange for Ca, which is released from the rock into the fluid (Alt, 1995; Berndt, 1987; Berndt et al., 1989; Mottl et al., 1974; Seyfried et al., 1988; Seyfried et al., 1991; Tivey, 2007; Wolery and Sleep, 1976). This reaction can be stated generally as:

$$CaAl_2Si_2O_8 + 2Na^+ + 4SiO_{2(aq)} \Rightarrow 2NaAlSi_3O_8 + Ca^{2+} \qquad (10)$$

Note the removal of Na and addition of Ca during the formation of albite. Near the magma chamber, acidic magmatic fluids and magmatic volatiles (H_2O, CO_2, SO_2, H_2S, H_2, He), can be introduced to the newly evolved hydrothermal fluids, along with very high temperature reactions of the new fluid with host rocks, including deposition of magma-derived SO_4 as anhydrite, titration of acidity, and further metal mobilization (Craig and Lupton, 1981; Gamo et al., 1997; German and Von Damm, 2003; Hannington et al., 2005; Lupton et al., 2008; Reeves et al., 2011). Subsequently, both "supercritical" and "subcritical" phase separation can occur. Above the critical point, "supercritical" phase separation can occur and create a high-salinity vapor (≥3.2 wt% NaCl) by

condensation of a small amount of liquid (Alt, 1995; Bischoff and Rosenbauer, 1985; Foustoukos and Seyfried, 2007; German and Von Damm, 2003). Recent evidence suggests that supercritical fluids occurring near a magma chamber can 'compact' without crossing the two-phase solvus (i.e., do not boil), thus creating very high salinity fluids crucial for development of high sulfide epithermal mineral deposits (Hedenquist and Lowenstern, 1994; Heinrich et al., 2004). However, subcritical phase separation below the critical point of seawater occurs as a result of decompression during upflow, wherever the 2-phase boundary is intercepted, producing ~3.2 wt% NaCl liquid coexisting with a low-salinity vapor (Berndt et al., 2001; Foustoukos and Seyfried, 2007; Seyfried et al., 2003). This process is essentially boiling, creating a gas-rich vapor phase and residual brine. Phase segregation, or separation of the low salinity vapor from the high salinity brine, can occur, which plays a crucial role in creating the large range of chlorinities often observed in hydrothermal fluids (Butterfield et al., 1990; Edmonds and Edmonds, 1995; German and Von Damm, 2003; Ishibashi, 1995; Tivey, 2007; Von Damm et al., 2003). Resulting brine phases are sometimes not able to ascend due to their high density (Alt, 1995), ultimately leading to a 'layered' hydrothermal system ("double-diffusive convection"; Bischoff and Rosenbauer, 1989; Butterfield and Massoth, 1994; Nehlig, 1993). In this case, fluids in the lower, denser layer recirculate and become more concentrated, while the upper layer has a 'single-pass' mixing with seawater (Bischoff and Rosenbauer, 1989). Rapid upflow of hydrothermal fluids occurs in the upflow zone, and can create both focused or diffuse discharge (note: 'diffuse' in this sense indicates vent fluids are not sufficiently channeled or focused to reach the seafloor directly while focused fluids indicate direct discharge of fluids from the subsurface reservoir; Alt,

1995). Focused flow is often accompanied by formation of epidosite (Alt, 1994; Nehlig, 1993). Secondary acidity can be generated by Fe sulfide deposition in both diffuse and focused upflow zones, and quartz precipitation is abundant (Alt, 1995; German and Von Damm, 2003; Hannington et al., 2005). During diffusive upflow, more mixing with overlying seawater occurs. Heating of this entrained seawater can cause deposition of admixed seawater SO_4 as anhydrite. If fluids fall below anhydrite stability temperatures, dissolution of previously formed anhydrite deposits can occur (Tivey, 2007). Additional low temperature water/rock reactions, such as boron fixation, may also occur prior to venting at the seafloor (Alt, 1995; Reeves et al., 2010). Mineral precipitation can occur upon cooling and due to redox reactions, which further removes some ions such as Si, Fe, and Mn very near the seafloor.

The identification and description of these processes are primarily from deep-sea hydrothermal vents. Much less is known about the subsurface processes taking place at shallow-sea hydrothermal vents. Although many of the processes occurring at deep-sea vents also occur in shallow-sea hydrothermal environments (Price et al., 2012), shallow-sea vents are by their very nature discharging at substantially lower pressures than those commonly found in deep-sea environments (Fig. 4). As a result, free gas phases are common in shallow-sea vent systems (Dando et al., 1995). This may lead to enhanced gas exsolution (formation of free gas bubbles or degassing)(e.g., Caracausi et al., 2005; Lupton et al., 2008), and may therefore substantially alter fluid chemistry by mass transfer from gas to aqueous phase (e.g., CO_2, H_2S scrubbing). Finally, it is important to note that most shallow-sea vent systems, including Panarea, are associated with arc volcanoes. These felsic-hosted magmatic hydrothermal systems contain more degassed

volatiles than their mid-ocean ridge counterparts. This can lead to much more acidic fluids, and subsequent leaching of Mg from host rocks (Reeves et al., 2011; Yang and Scott, 1996). These characteristics make shallow-sea hydrothermal venting distinctly different from their deep sea counterparts. Here we evaluate the potential subsurface processes taking place at Panarea, leading to an improved model for the evolution of the hydrothermal fluids. As a reference, we illustrate the main processes outlined above in Fig. 5.

5.1 General observations and mixing trends

The major element chemistry of vent fluids at Panarea suggests that a variety of subsurface processes may contribute to the geochemistry of each of the investigated sites. The Mg and SO_4 concentration for all samples are shown in Fig. 6a. For reference, horizontal and vertical lines indicate seawater concentrations of SO_4 and Mg, respectively. These data indicate that many, but not all, hydrothermal fluids analyzed during this study are depleted in Mg and SO_4 relative to seawater. Furthermore, the covariation between Mg and other major elements indicates a 'triple trend' mixing pattern (Figs. 6b and 6h). Enrichment of most major cations and anions occurs within (1) the Hot Lake pore fluids, (2) the focused vent fluids from Black Point, and (3) the gas-rich fluids from La Calcara, while La Calcara and Black Point pore fluids do not follow this pattern of enrichment (Table 1). Furthermore, mixing between seawater and the Hot Lake fluids is different when compared to Black Point vent fluids and La Calcara gas-rich fluids (Figs. 6b-6h). The regression line connecting the seawater value and Hot Lake fluid data points is much steeper when compared to the other two sites, and as such

suggests the possibility for a much higher salt content as a source fluid. Thus, there must be more than one hydrothermal end-member for the vent fluids, and the pore fluids collected from Black Point and La Calcara, although high temperature and low pH, evolved in a different manner than the other fluids.

As defined by the disparate mixing trends, all the fluids measured during the course of this study can be categorized into three major groups. The fluids most enriched in major elements relative to seawater (i.e., the Hot Lake pore fluids), are regularly referred to as 'Type 1' fluids. The vent fluids from Black Point, along with gas-rich fluids from La Calcara, follow similar compositional trends and are therefore labeled as 'Type 2' fluids. In contrast, pore fluids from Black Point and La Calcara, which do not generally show enrichments of major cations and anions, will be referred as 'Type 3' fluids. These distinctions allow for the identification of mixing trends with seawater and separate hydrothermal end-members.

5.2 Subsurface evolution of hydrothermal fluids

5.2.1. The End-members

The subsurface evolution of the hydrothermal fluids at Panarea can be investigated by calculating the end-member hydrothermal reservoir composition(s), which is often carried out assuming a Mg concentration of zero in the hydrothermal end-member (the "zero-Mg" extrapolation method; Bischoff and Disckson, 1975; Mottl et al., 1974). This assumption is made on the understanding that Mg should be almost entirely removed from the hydrothermal fluids as a result of water-rock interactions above ~150 °C. Unlike most deep-sea submarine hydrothermal vent fluids, Mg and SO_4 do not

extrapolate to zero concentration for the Panarea fluids (see projected intercept on Fig. 6a). Vent fluids have sulfate concentrations below what would be expected for simple seawater mixing. This may be due either to sulfate reduction or precipitation of anhydrite below the seafloor (Butterfield and Massoth, 1994). Most fluids extrapolate to SO_4 = zero at ~30 mM Mg (Fig. 6a), although two Type 2 vent fluids extrapolate to zero-SO_4 at zero-Mg. The negative sulfate intercepts are most likely due to some seawater entrainment into the near-seafloor plumbing system resulting in sulfate removal as anhydrite, while Mg remains in solution and is vented (i.e., seawater entrainment at temperatures high enough for anhydrite to precipitate but not high enough for water-rock interactions to remove all Mg (Butterfield and Massoth, 1994)). Given the abundant anhydrite present within Panarea sediments (see later discussion), this is a likely scenario. This would furthermore explain why only the very high temperature fluids have SO_4 depletion relative to Ca (Table 1). Following this line of thinking, using Mg = 0 is still a valid assumption.

5.2.2. Subsurface Processes

In Table 2, we report the calculated hydrothermal end-members based on Mg = 0 mM in the deep hydrothermal reservoir fluid. In the case of most pore fluids for Black Point and La Calcara, concentrations are too close to seawater in composition to accurately determine the end-member, and thus mostly only Type 1 and Type 2 fluids are reported. Our calculations confirm that the hydrothermal reservoir fluid feeding Hot Lake has a much higher salt content overall after removing the seawater component (Table 2). For example, Hot Lake Na concentrations ranged from 471-1113 mM (mean 960; n = 20), compared to 444-463 (mean 452; n = 3) and 306-317 (mean 312; n =2) mM for

Black Point and La Calcara vent fluids, respectively (Fig. 7a). Calcium concentrations were a mean of 570 mM at Hot Lake, compared to a mean of 150 and 112 mM for Black Point and La Calcara, respectively (Fig. 7b). The higher salt content of the reservoir feeding Hot Lake is also reflected in K, B, Sr, and Br end-member data (Table 2). Chloride concentrations are exceptionally elevated in concentration (Tables 1 and 2; Figs. 7a-7b), and chloride end-member concentrations reach a mean value of 2220 mM for Hot Lake fluids, and 847 and 532 for Black Point and La Calcara, respectively. In comparison to other systems (e.g., mid-ocean ridge and back-arcs), the Panarea concentrations are much higher. For example, in Figs. 7a-7b, typical end-member concentrations of Na and Ca in various hydrothermal systems are plotted. Not only do Na values for Hot Lake (Type 1) fluids reach higher values, but Cl concentrations are more than double that typically calculated for any other deep-sea hydrothermal system.

As described at the beginning of the discussion and illustrated in Fig. 5, several processes can contribute to these compositions. Experiments have shown that often the observed salinities in hydrothermal vent fluids cannot solely be explained by phase separation (Bischoff and Rosenbauer, 1987), and it was suggested that the observed variations in mid-ocean ridge hydrothermal fluids could only be explained if seafloor geothermal systems consist of two vertically nested convection cells (Bischoff and Rosenbauer, 1989). The lower cell, composed of highly saline brine, circulates at depth within the cracking front and transfers heat and some salt to the overlying seawater (single pass) cell during double-diffusive convection (this is illustrated in detail in Fig. 5). If the hypothesis of a double-diffusive deep recirculating brine is true, then one could

imagine all elements in this zone could be further enriched through distillation over time. This could explain the 'extreme' concentrations of major elements in Type 1 fluids.

For most mid-ocean ridge fluids, the Na/Cl ratios for vents with elevated chlorinity are not scattered but define a reasonably straight line that departs from the seawater evaporation trend with lower Na, and the relative Na deficiency with increasing Cl is made up primarily by increasing Ca (Bischoff and Rosenbauer, 1989). We observe a similar trend for the Panarea data (Table 2 and Figs. 6a-6b). These data indicate two co-occurring phenomena: first, Cl enrichment as a result of the concentrating effect of the phase separation (see below) and the formation of a double-diffusive, recirculating brine deep reservoir, and second, Na/Ca variation as a result of water-rock interactions (Fig. 5). Sodium can be removed from the fluids as a result of Na–Ca replacement reactions in plagioclase feldspars, i.e., albitization. On a chloride-normalized basis, Na is decreased in hydrothermal fluids relative to seawater, suggesting Na removal (Table 2). On the other hand, Ca, K, and Sr are higher relative to seawater (again, on a Cl-normalized basis), suggesting enrichment of these elements. Low Na/Cl and high Ca/Cl fluid ratios relative to seawater can be inferred to be caused by albitization (Gallant and Von Damm, 2006). The observed Na/Cl and Ca/Cl ratios in the Panarea fluids follow this trend, although they plot separately from most deep-sea systems, particularly for Type 1 fluids (Fig. 7c). This suggests that significant replacement of Na with Ca is occurring, particularly for Type 1 (Hot Lake) fluids (Figs. 7a-7c). However, because the ratios fall on more or less the same trend as other vents, it is likely that these elements are concomitantly enriched in the brine reservoir. Furthermore, the deviation of the data for Panarea (more Ca, less Na), is most similar to that observed for other arc- and back-arc related hydrothermal

systems, relative to mid-ocean ridge systems (Figs. 7a-c). Strontium is, like Na and Ca, solubility controlled (Berndt et al., 1988), and the Sr/Cl ratios reflect similar trends in the Type 1 fluids (Fig. 7d). High Ca concentrations and low Sr/Ca also provide evidence for albitization because Sr is partitioned strongly into albite; fluids which have formed Na-rich plagioclase should have a lower Sr/Ca ratios (Butterfield and Massoth, 1994).

The co-variation between the Sr concentrations and the $^{87}Sr/^{86}Sr$ for selected fluid samples from this study and Panarea volcanic rocks (igneous rocks from the surrounding islands; Calanchi et al., 2002), are displayed in Figure 7c. Also included for comparison are values from a locally deposited volcanic ash layer, which can reach up to 9.5 m thick on Panarea Island (Calanchi et al., 2002; Calanchi et al., 1999), and vent precipitates associated with the Black Point chimney edifice (unidentified but possibly "strontiobarite" or related metal sulfides; Becke et al., 2009; Sieland, 2009). As pointed out above, the basement rocks of Panarea are actually somewhat heterogeneous, having transitional compositions between the western and eastern arc (Calanchi et al., 2002). We've highlighted the $^{87}Sr/^{86}Sr$ and 1/Sr fields for these rocks, noted as "Stromboli Affinity" and "Western Arc Affinity" in Figure 7e. This suggests that the hydrothermal fluids at Panarea are equilibrated more with the rocks of Stromboli affinity. The ash layer is reported to consist of glassy calc-alkaline basalt to basaltic-andesite, plus a thin interbedded trachytic ash with potassic-alkaline character, possibly sourced from nearby Stromboli volcano (Calanchi et al., 1999).

The $^{87}Sr/^{86}Sr$ ratio and Sr concentrations depend on the extent of water/rock interaction as function of temperature and bedrock lithology (Berndt et al., 1988). Laboratory experiments consisting of diabase and seawater at 375-425°C and 375-400

bars produced dissolved Sr/Ca ratios in close agreement with those observed in ridge crest hot springs, while basalt alteration produced ratios that were much lower. This suggests that interaction of hydrothermal fluids with diabase deeper in the hydrothermal system – not basalt in the shallower areas – at high temperatures is a good analog to subsurface processes responsible for production of ridge crest fluids (Berndt et al., 1988). This suggests that most hydrothermal fluids in mid-ocean ridge environments are obtaining their compositions deep in the ridge system. The general trends observed for Panarea fluids suggest a similar trend, and therefore deep-seated reactions may dominate the overall evolution of the fluids.

5.2.3. Phase separation vs. Degassing

Previous investigators have suggested the possibility of phase separation at Panarea (e.g., Sieland, 2009; Tassi et al., 2009). Most of the Type 3 fluids have Cl values less than seawater (Table 1), and a plot of Cl vs. Na suggests that (subcritical) phase separation and phase segregation may have occurred (Fig. 8a). We note in this figure also that the fluids with Na and Cl less that seawater concentrations trend towards a zero concentration, and that above seawater concentrations the decrease in Na is again obvious, suggesting Na removal. Chloride and Br are typically thought to be little affected by water-rock interactions. Figure 8b indicates that these two elements linearly correlate (r^2 = 0.99 for all data points), but that concentrations for both can be below seawater values, and extend to zero. Bromide, as viewed through the Br/Cl ratio, can be fractionated from chloride whenever halite is formed or dissolves, because bromide is preferentially excluded from the halite structure (the ratio increases during halite

precipitation, but decreases halite dissolution; (Oosting and Von Damm, 1996; Von Damm, 2000). Fluids that have precipitated halite will therefore have high Br/Cl ratios, while fluids that have dissolved halite will have low Br/Cl ratios, relative to seawater. Measured values for Cl vs. Br/Cl indeed show significant deviation of the Br/Cl relative to seawater (Fig. 8c). However, organic matter degradation has been shown to increase Br concentrations to as much as 2.9 times seawater value, which can thus change the Br/Cl concentration relative to seawater (Martin et al., 1993). Alteration of volcaniclastic sediments can also alter the Br/Cl ratio (Martin, 1999). End-member Cl vs. Br/Cl ratios suggest that departures from the Br/Cl ratio of seawater can occur for Panarea hydrothermal fluids, although not significantly (Fig. 8d). This occurs for one Hot Lake fluid, and most of the La Calara and Black Point fluids. It is important to note that most Type 3 fluids calculated to negative values for Cl and Br (i.e. Cl and Br = 0). For these fluids the Br/Cl ratio would be zero, although for several of the Black Point Type 3 fluids, the bromide concentrations ranged from 0.1 to 0.4 mM. The Br/Cl ratio for these fluids would be above that for seawater, suggesting that, although we cannot plot these values, phase separation cannot be discounted.

Finally, if phase separation is occurring, the vapor phase should be enriched in neutral aqueous species reflecting the low-ionic strength of the solution and the associated salting-out effects in the highly ionic brine phase (Foustoukos and Seyfried, 2007). In this case, B/Cl ratios will tend to increase with Cl decrease due to the vapor enrichment in $B(OH)_{3(aq)}$. If the fluids from Black Point and La Calcara (Type 3) reflect the input of a low-salinity vapor phase, then the B/Cl molar ratios in these samples should

be larger than others. We only see evidence for this in one sample (Fig. 8e). Again, this suggests that phase separation is not a major process in the subsurface at Panarea.

However, invoking a lack of phase separation is problematic because it does not help explain the occurrence of the deep recirculating brine (the source of Type 1 fluids). It could be hypothesized that this brine may have been created by phase separation, followed by distillation and a continuing increase in salt content, but the Br/Cl and B/Cl ratios do not support this hypothesis. It is possible that this deep brine was generated by 'compaction' of supercritical fluids without crossing the two-phase solvus (i.e., does not boil; Hedenquist and Lowenstern, 1994; Heinrich et al., 2004). This, theoretically, could create the Type 1 fluids without deviations from the Br/Cl and B/Cl ratios. However, without more data we can only speculate at this time.

Type 3 fluids are hot and acidic, but have salinities that are near to that observed for seawater. One possible explanation is that seawater is being altered by the abundant free gas present in the system. Dissolved gases (CO_2, H_2S, etc.) are primarily present in vent fluids from magmatic volatile inputs. These dissolved gases can come out of solution to form free gas bubbles in two ways, both of which occur as a result of depressurization. The processes are: 1) boiling (i.e., sub-critical phase separation), and 2) exsolution, or phase transition from an aqueous to a gas phase (e.g., $CO_{2(aq)} => CO_{2(g)}$). Exsolution is a chemical process that occurs during (subcritical) phase separation (including boiling), while phase separation is caused by changes in physical conditions. Dissolved volatile species (H_2, H_2S) have a strong tendency to partition in the vapor phase during subcritical phase separation, but phase separation need not occur for free volatiles to form. While phase separation will always be accompanied by exsolution if the

parent fluid contains dissolved magmatic gases, exsolution does not require phase separation, only depressurization. As we have noted above, shallow-sea vent systems allow for depressurization without phase separation (Fig. 5). Exsolution, with or without phase separation, can result in scrubbing of those gases (e.g., CO_2 to create carbonic acid, SO_2 to create sulfide and sulfuric acid), delivering heat and other dissolved constituents which alter the fluid composition. Gas absorption or scrubbing involves the re-distribution of solutes between the gas and the liquid phase when the 2 phases come into close contact with each other (Delalande et al., 2011; Kenig and Górak, 2005; Rouwet and Tassi, 2011). However, some steam condensation must be involved to obtain the observed dilutions. Most likely, these processes co-occur. We therefore suggest that this phenomenon plays a key role in influencing the composition of Type 3 fluids. They are sediment pore fluids (i.e., buried and entrained seawater) which have been altered by mass transfer from free gas bubbles derived from depressurization release from the dissolved phase.

Although less common in deep-sea hydrothermal systems, free gas bubbles are nearly always present in shallow-sea hydrothermal systems due to lower pressures. Note that the P-T conditions for shallow-sea vents in Fig. 4 suggest this will be controlled primarily by changes in pressure, rather than temperature. The gases in the Panarea hydrothermal system are predominantly CO_2, H_2S, and trace O_2, N_2, CO, and CH_4 (Italiano and Nuccio, 1991). This is within typical values for shallow sea vent gases investigated to date (Dando et al., 1995; Italiano and Nuccio, 1991; Pichler et al., 1999). Thus, this phenomenon may be ubiqutious in shallow-sea vents, and evolution of Type 3 fluids may therefore be common in shallow-sea hydrothermal systems. Continuous gas-

liquid exchange in shallow-sea vents can create a new type of hydrothermal fluid, which is hot and acidic due to exchange of heat, CO_2 and H_2S, but which has close to seawater major ion concentrations. Small amounts of water vapor condensation will create slight dilutions in major ion chemistry of the sediment pore fluids. Furthermore, if the heat from these gases bubbling through seawater raise the temperatures to above ~130 °C (e.g., as observed for the shallow sediments at La Calcara and Black Point), anhydrite precipitation can occur, removing SO_4 but not Mg.

5.2.4. Secondary Processes

We note that some Mg values are higher than seawater, although concentrations are only slightly higher (<2 mM), and only for some of the Type 3 fluids (Fig. 5a). It has been suggested that higher than seawater Mg in hydrothermal fluids may possibly occur as a result of acid leaching of Mg from host rocks in arc/back-arc systems where the pH is exceedingly low (Gamo et al., 1997; Reeves et al., 2011; Resing et al., 2007). We hypothesize that acid alteration is causing the Mg enrichments in Panarea fluids. Argillic alteration occurs in highly acidic, often high sulfide conditions characteristic of near-seafloor (or near-surface) hydrothermal environments where oxidation H_2S (or SO_2) produces sulfuric acid (Shanks III, 2012). Magnesium is often depleted in rocks from these zones, while K is enriched (Lowell and Guilbert, 1970; Pirajno, 2009; Shanks III, 2012; Tivey, 2007), suggesting the Mg enrichment should occur in resulting fluids. Alunite ($KAl_3(SO_4)_2(OH)_6$), a common product of argillic alteration, is common in Panarea sediments (Dekov et al., 2013; Prautsch et al., 2013), and during sampling abundant white clay materials were often observed in the lower portions of cores (~10-30

cm depth). As high temperature gases (primarily CO_2 and H_2S) move through sediment pore fluids, carbonic and sulfuric acid is produced. Thus, Mg is replaced by K in these shallow rocks and sediments, and Mg enrichment occurs. This furthermore helps explain lower K values in these fluids (Table 1).

Anhydrite precipitation may be a major influence on the composition of discharging fluids. Preliminary scanning electron microscopy (SEM) combined with energy dispersive X-ray analyses were carried out on hard precipitates found at the La Calcara gas-rich area. The results, shown in Figure 9a, reveal the first discovery of massive anhydrite deposits at the sediment/seawater interface in a shallow-sea hydrothermal system. Measured Ca vs. SO4 for Type 3 fluids trend from seawater values to zero concentration for each, suggesting complete removal of these elements (Fig. 9b). The first step in the formation of a deep-sea black smoker chimney is precipitation of an anhydrite framework caused by the heating of seawater as hydrothermal fluids first begin to discharge (Haymon, 1983). Anhydrite solubility (Ω), as a function of temperature using seawater as the starting fluid, was calculated by dividing the ion activity product (IAP) by the solubility product (Ksp) for the reaction of Ca^{2+} with SO_4^{2-} to produce $CaSO_4$. Data indicate that above ~100 °C (at saturation pressure), anhydrite becomes insoluble (Fig. 9c). Because the hydrothermal vent fluids observed at both Black Point and La Calcara were approximately 135 °C, anhydrite precipitation is expected in the shallow subsurface environments, although Ca appears to still be present in these fluids (Fig. 9b). This scenario could have led to the current "chimney" at Black Point. The high temperature site at La Calcara was not observed prior to 2009, but was present during both the 2009 and 2010 expeditions, suggesting that a chimney-type structure may be

forming there. Widespread anhydrite precipitation in the subsurface sediments surrounding the submerged caldera off Panarea was observed during drilling at the site, which revealed abundant massive anhydrite/gypsum as well as native sulfur. These precipitates were interpreted to represent a cap forming at the interface between seawater and geothermal fluids ascending towards the seafloor (Petersen et al., 2007).

Minor or trace elements, such as Si, Fe, Mn, Ba, Li, Rb, and Cs are also useful tracers of hydrothermal input because their concentrations are even lower in seawater. Concentrations of these elements compared to that of Mg illustrate the differences between each site investigated for this study. For example, several of the trace elements follow similar patterns as observed for K, Na, B, Sr, and Br vs. Mg and SO_4 (specifically, Mn, Ba, Li, Rb, and Cs are enriched only in Type 1 and 2 but not Type 3 fluids; Figs. 10a-10e). This suggests solubility controls on these elements. Silica is most elevated in the lowest Mg samples, particularly for Hot Lake (Fig. 10e). Furthermore, Black Point vent and pore fluid concentrations are elevated in dissolved silica, despite having near seawater Mg concentrations. Elevated silica concentrations in hydrothermal fluids are common, as silica is readily leached from the rocks hosting the hydrothermal fluids, and will only be removed upon cooling and precipitation (typically as silica sinter). Iron, in contrast to silica, is relatively low in all Black Point and Hot Lake fluids, while La Calcara Fe concentrations are much more elevated (Fig. 10f). Elevated Fe concentrations at La Calcara are not unexpected, as precipitates of Fe-(oxy)hydroxides are abundant.

5.3. Hypothetical Model

A model of subsurface processes at Panarea was first proposed by Italiano and Nuccio (1991), and has since been suggested by others (Caracausi et al., 2005; Tassi et al., 2009; Sieland, 2009). Fluids were hypothesized to be derived from a high-Cl reservoir recharged from very deep in the system, and an overlying shallower, medium salinity reservoir (higher salinity relative to seawater but considerably lower salinity compared to the deeper high-Cl portion). We suggest here that the deeper high Cl reservoir could have been created by 1) direct condensation of a supercritical phase, and/or 2) double-layered convection, and the development of a closed, recirculating brine cell. Our data suggest that the Type 1 (Hot Lake) fluids are discharging from the deeper high-Cl reservoir directly to the seafloor. Overlying the deep brine cell, seawater is circulating through in a 'single-pass' system, thus diluting the higher element concentrations found in the deeper reservoir. Type 2 (Black Point vent and La Calcara gas-rich) fluids are being fed by this shallower reservoir. Finally, Type 3 fluids develop as dissolved gases exsolve at depth and rise rapidly to the surface, bringing heat, CO_2 and H_2S. This heat and gas is then transferred to sediment pore fluids near the composition of seawater. Each of these processes are illustrated in Fig. 5, which shows the special character of shallow-sea hydrothermal venting.

5.4 Catabolic potential

5.4.1 Overview and Approach

As illustrated by the trends outlined and discussed in the preceding sections, variability in the geochemistry of discharging fluids exists as a function of the mixing of seawater with different types of hydrothermal end-member fluids. This will ultimately

influence the microbial communities at each specific site through the availability of potential electron donors derived from each fluid type, and electron acceptors mainly derived from seawater.

In order to evaluate the theoretical spectrum of potential metabolic energies encountered at the Panarea sites, we selected data from two samples from each of the vent sites which represent both a high and moderate temperature for our energetics calculations. These samples also represent variability in fluid types encountered in the system. Temperature, along with Mg concentration, is one of the best ways to track hydrothermal fluid mixing with seawater. In this case, one fluid contained low levels of Mg (35 to 41.5 mM) and therefore represented fluids characterized by a relatively large hydrothermal fluid component (i.e., higher T), and the other was characterized by mid-range Mg levels (46.7 to 55.5 mM), more similar to seawater (lower T). The samples selected are highlighted in grey in Table 1, and indicated by a star in Figure 5a.

In order to quantify the potential metabolic activity of the hydrothermal system off Panarea Island, the Gibbs energies of the 61 reactions listed in Table 4 were calculated. These reactions contain all of the electron donors and acceptors that were measured during field expeditions during 2008-2010. However, in order to be able to calculate the potential metabolic activity at the site, we also included values not measured in this study (e.g., H_2, CH_4, O_2, CO_2, CO, NH_4^+), but that have been reported in other studies that were sampled from the same exact sites (Luther and Tsamakis, 1989; Müller, 2011; Sieland, 2009; Tassi et al., 2009; and the National Institute of Geophysics and Volcanology, Palermo (INGV)). For example, values for seawater concentration of Mn are from Klinkhammer et al. (1985). The iron concentration in seawater is taken to be the

equilibrium value calculated using Geochemist's workbench. In order to accurately calculate the Gibbs energies of these reactions, the in situ activities of the species in them were determined by carrying out speciation calculations at the temperature of interest using the concentration data given in Tables 1 and 3 and Geochemist's Workbench using the thermo.dat dataset. Seawater values for aqueous H_2S are from Luther and Tsamakis (1989). Aqueous seawater values for CH_4, H_2, CO, and N_2 are from Charlou et al. (2002). NO_3^- values at Hot Lake and La Calcara is an average of values from Tassi et al. (2009). Because dissolved O_2 at La Calcara was not reported, the equilibrium value for O_2 free gas concentrations were used. NO_2^- at La Calcara is an average of the other sites. Available data for Hot Lake, Black Point, and La Calcara (e.g., HCO_3, O_2, NO_3, NO_2, NH_4, Fe, and Mn) are from Sieland (2009), Müller (2011), and Tassi et al. (2009).

Ideally, the concentration of all the reactants and products in the metabolic reactions would have been taken from the exact same samples in order to characterize the energetic potential of a particular fluid at a precise moment in time. However, these data were not collected, and excluding reactions containing these species would not accurately represent the metabolic potential of Panarea hydrothermal vents since they are known to exist there. Our first assumption is that some of these species (e.g., free gas phases, CO_2, H_2S, etc.), do not have significant temporal and/or spatial differences relative to the sampling. These data have been consistently similar, with very little difference in the gas compositions, over the past several decades (Italiano and Nuccio, 1991; Italiano, pers. comm), and we therefore consider this to be a safe assumption. It is clear that some dissolved species (e.g., HCO_3, NH_4^+, etc.) will change with mixing ratio between seawater and hydrothermal end member. For these data, we matched the fluid

temperatures and Mg concentrations reported in the literature with the measured temperature and Mg concentration for the sample chosen for the calculations. Despite these shortcomings, we consider the data set is adequate enough to allow us to estimate the potential metabolic activity at each site.

5.4.2. Energetics per electron transferred

The Gibbs energies of the 61 reactions listed in Table 4 are shown in order of exergonicity in Figures 11a and 11b. Each horizontal bar in these figures represents the calculated range of ΔG_r available from the indicated reaction for the temperature and chemical composition conditions of all six of the sample sites listed in Table 3. The color of the lines in Figures 11a and 11b indicates the type of electron acceptor (oxidant) and donor, respectively, in each reaction (as shown in the legend). The variable lengths of the bars are due to the stoichiometry of the reactions under consideration and the variable temperatures and compositions of the six study sites. As has been shown in similar energetic profiles (Amend et al., 2003b; Rogers and Amend, 2005; Rogers and Amend, 2006; Rogers et al., 2007; Shock et al., 2005; Shock et al., 2010), the range of ΔG_r spans from approximately 0 to -120 kJ (mol e-)$^{-1}$. Disproportionation reactions and those in which S^0, SO_4^{2-}, CO and CO_2 serve as oxidants are among the least exergonic reactions, typically less exergonic than -20 kJ (mol e-)$^{-1}$. However, it is worth noting that some of the reactions in which O_2, NO_2^-, NO_3^-, N_2, Fe(III), and Mn(IV) serve as electron acceptors also fall into the low end of the energy spectrum, despite their reputation for being highly exergonic oxidants (LaRowe and Van Cappellen, 2011). In fact, the energetics of those reactions in which these species are oxidants are found throughout the

range of Gibbs energies shown. Therefore, knowledge of the electron acceptor does not necessarily indicate the energetics, and thus the likelihood, of a given metabolic strategy being utilized in a particular setting.

5.4.3. Energy density

The exergonicity of potential catabolic strategies shown in Figures 11a and 11b can give a somewhat misleading impression of which reactions are most energetically relevant to microorganisms in a particular environment. For instance, the three most exergonic reactions shown in Figures 11a and 11b all have nitrite as an oxidant. However, the concentration of nitrite at the six samples sites is micromolal or less (and is expected to be so regardless of the data source). A more considered approach is to normalize the potential energy per kilogram of H_2O (e.g., (McCollom, 2000; LaRowe and Amend, 2014). The result of using this method is illustrated in Figures 11c and 11d, where the range of energy available per kilogram of H_2O for the 61 reactions shown in Table 4 at the temperature and chemical composition conditions of all six of the sample sites are plotted. The horizontal bars refer to the energetics of reactions in the same order as those shown in Figures 11a and 11b. It can be clearly seen that the most exergonic reactions reported per mole of electron transferred in Figures 11a and 11b are not the most energy-rich reactions when presented as per kilogram of H_2O. Metabolisms that rely on nitrite as an electron acceptor are not substantial sources of energy. Additionally, some of the least exergonic reactions in Figures 11a and 11b, e.g., those in which Fe(III) and Mn(IV) are the oxidants, provide far more energy per kilogram of H_2O than those that appear to be the most exergonic per mole of electron transferred. The values of E_{H_2O}

with the lowest energy yield for each reaction were used to generate Figures 11c and 11d, since in most cases either the electron donor or acceptor will be a limiting reactant. In order to carry out these calculations the activities of all reactants and products were held constant, simulating a steady state condition. The energetics of the disproportionation of S^0 (Reaction 37) was not included in this analysis since there is no limiting species other than the presence of S^0.

The amount of energy available varies by several orders of magnitude, as indicated by the length of the bars in Figures 11c and 11d. This is due to the broad range of methane concentrations at the sample sites. It is noteworthy that the amount of energy available from the oxidation of methane by O_2, NO_3^-, NO_2^-, goethite, pyrolusite, S^0 and SO_4^{2-}, per kg of H_2O, can all generate equivalent amounts of energy, depending on the site. In fact, in terms of oxidants, only SO_4^{2-}, (Reactions 9 and 10) is not capable of producing more energy than O_2 through the oxidation of CH_4. Per kg of H_2O, there is somewhat less energy available from reactions in which H_2 is an electron donor than that for CH_4. Also, there is a narrower range of energies derived from H_2 at the study sites than from methane. However, all of the H_2 oxidation reactions (except Reaction 23) can supply as much energy as O_2 (Reaction 12), which is similar to CH_4. Because the abiotic rate of the knallgas reaction is faster at higher temperatures (Foustoukos et al., 2011), we might expect that in the hottest hydrothermal systems, microorganisms would have to be able to catalyze the knallgas reaction (Reaction 12) faster than it happens abiotically. However, the concentrations of H_2 and O_2 used in this study are measured values of these species in this system and therefore the resulting energetics calculations are a direct reflection of the energetic potential of this system, which is our goal. The knallgas

reaction is not anywhere close to being a major supplier of energy when normalized to J / kg of H_2O, so we have opted to leave out further discussion of the biotic vs. abiotic rates of the knallgas reaction.

The most consistently energetic class of reactions per kg of H_2O is those involving the oxidation of H_2S and S^0, shown in Figures 11c and 11d. That is, Reactions 24-37 supply nearly 1 J / kg H_2O or more at one or more of the sample sites. Furthermore, Reactions 24-27 and 31-34 supply > 10 J / kg H_2O at one or more of the sample sites. By presenting the energetics of these reactions per kg of H_2O, it can be seen that sulfur oxidation (H_2S and S^0) is likely a major source of energy for microorganisms living in the hydrothermal systems at Panarea.

The energetics of Mn^{2+}, NH_4^+ and Fe^{2+} oxidation by various electron acceptors, Reactions 38-50, are also shown in Figures 11c and 11d. Ferrous iron oxidation provides a moderate range of energies at the six sample sites, between about 0.01 and 0.5 J / kg H_2O. Interestingly, the oxidation of NH_4^+ by MnO_2, Reactions 43 and 44, are the most energy yielding reactions considered in this study per kg H_2O, due mostly to the high concentrations of ammonium at some of the sites. For the same reason, the oxidation of Mn^{2+}, Reactions 38-40, could be moderate sources of catabolic potential, although they are not as rich in energy.

Oxidation of CO is generally a highly exergonic reaction per mole of electron transferred. However, when considered per kg of H_2O, it is among the least energy rich electron donors in Panarea hydrothermal fluids due to its low concentration, regardless of the oxidant (Reactions 51-59, see Figures 11c and 11d).

NH_4^+ oxidation provides more energy than H_2S and S^0 (Figures 11c and 11d) at most sites. The highly exergonic NH_4^+ oxidation reactions are with MnO_2 as the oxidant (Reactions 43 and 44). These reactions are highly exergonic primarily due to the fact that, because MnO_2 is a mineral, it does not have a limiting concentration (i.e., the activity is taken to be 1). However, when the same calculations are conducted for H_2S, which also has high concentrations, the lower-concentration oxidants become the limiting reactants, resulting in less energy per kg H_2O. Thus, while NH_4^+ oxidation by MnO_2 appears to be a dominant metabolism, this is unlikely. This is because this bioenergetic calculation assumes the presence of MnO_2, but this mineral is clearly not present in, for example, the Hot Lake fluids. Thus, it is unlikely that Reactions 43 and 44 are a dominant metabolism utilized by the microorganisms at Panarea (i.e., the reactions of Mn-reduction should not occur because of the absence of MnO_2 minerals).

5.4.4 Energetics comparison by fluid type

Figure 12 summarizes the energy available from the same groups of reactions containing the same electron donors but has the MnO_2 oxidation reactions removed from the figure. This indicates that reactions containing H_2S and S^0 are most likely to be the dominant metabolisms at each of the sites and fluid types investigated (note: reactions with very little available energy are omitted from this figure). Mn^{2+} oxidation provides some energy at each of the sites investigated. CH_4 oxidation could also be a potential source of metabolic energy for the La Calcara gas-rich fluids due to the elevated concentrations of this electron donor at this site (Table 3). Although iron concentrations

were elevated at La Calcara relative to the other sites, oxidation of Fe^{2+} does not provide a significant amount of energy (Fig. 12).

While H_2S and S^0 oxidation by O_2 is similar between Hot Lake and La Calcara sites (e.g., each produces ~40 J per kg of H_2O), these reactions for Black Point vents yield much more energy. This is due to higher O_2 concentrations in the Black Point fluids, which is likely the result of the hydrology of the shallow subsurface at Black Point (i.e., more seawater entrainment occurs in the shallow seafloor sediments at Black Point, and thus more O_2 exists in these fluids; Italiano and Nuccio, 1991). This may be the key controlling factor when comparing the bioenergetics of this system: seawater entrainment provides more O_2 at Black Point, which causes the electron acceptor to no longer be limiting. Thus, as noted, shallow, near seafloor seawater entrainment may be a crucially important phenomenon. Shallow-sea hydrothermal systems, with large fluxes of free gas, may enhance this seawater entrainment (Dando et al., 2000; Haeckel et al., 2007).

5.5 Comparison of available energy to microbial diversity and other sites

Several lines of evidence suggest that sulfur should be the predominant metabolized element in this system. For example, sedimentary sulfur isotope data indicate the presence and activity of different sulfur utilizing bacteria (Peters et al., 2011). Furthermore, chemolithoautotrophic, sulfur-oxidizing rod-shaped bacteria isolated from vent samples are “Thiobacillus-like” (Gugliandolo et al., 1999). Thiobacillus spp. display a wide range of metabolisms primarily associated with oxidation by O_2 of S or Fe (oxidation of H_2S by O_2 is common). Microscopic observation of a subsample from a whitish mat revealed a variety of morphologically distinct filamentous forms resembling

the Thiothrix genus, a filamentous sulfur-oxidizing bacteria (Gugliandolo et al., 2006). Those authors demonstrated that several of these strains deposited sulfur externally, and produced sulfate in liquid medium.

Recent molecular investigations at Hot Lake suggest that microorganisms making up the white filaments at the site are a highly diverse community of bacteria dominated by sequences of Epsilonproteobacteria (Berg, 2011). This is similar to deep-sea vent sites where, due to their ability to carry out different types of metabolism using a variety of alternate electron donors (e.g. H_2, formate, elemental sulfur, sulfide, thiosulfate) and acceptors (e.g. sulphite, elemental sulfur, nitrate), Epsilonproteobacteria play an important role in carbon, nitrogen and sulfur cycles. Members of the Thiotrichales order were not detected, which was surprising since they are commonly observed in marine sulfur mats. The archaeal clone library was less diverse: most of the archaeal sequences were related to thermophilic and hyperthermophilic organisms but no Crenarchaeota were found. Overall, the data suggest it is likely that elemental sulfur filaments in the white mats are biologically precipitated as part of a microbially-mediated sulfur cycle. Further evidence for S metabolism at the site is provided by cultured relatives of the detected species, which are mostly able to catalyze sulfur related metabolisms, including sulfide oxidation, sulfur reduction or sulfate reduction (Huang, 2012). Metagenome analysis supports the relevance of sulfur metabolism and of the rTCA cycle for autotropic life at Hot Lake (Huang, 2012). Maugeri et al. (2009), suggested that sulfur-oxidizing bacteria were detected by both culture-dependent and -independent methods at two nearby sites within the Panarea submerged caldera.

Thus, microbiological and genomic data support our interpretation that H_2S and S^0 oxidation seem to be the dominant metabolisms at each of the Panarea sites. This observation is similar to that for deep-sea vents where, in both the basalt-hosted and felsic rock-hosted systems, sulfide oxidation is the predominant catabolic energy source at all temperatures (and SW:HF ratios) considered (Amend et al., 2011). Differences in temperature do not influence the potential energy much at each site, but rather it is the concentrations of electron donors and/or acceptors, which play a larger role. Amend et al., (2003b) also made a similar observation for hydrothermal vent fluids collected from Volcano Island (Italy).

Most of the studies that have quantified the amount of energy available to microorganisms in natural settings only present results in units of energy per mole of substrate or electron transferred. As noted in the Introduction, the range of exergonic energy yields, for inorganic and organic redox reactions alike, fall between approximately 0 to -120 kJ per mole of electrons transferred. However, it is illustrated in Fig. 11 and elsewhere (LaRowe and Amend, 2014; Osburn et al., 2014) that energetic yields normalized per mole of electrons transferred can predict a very different set of reactions that are likely being catalyzed than energetics calculations that take into account the concentrations of limiting reactants as well. In order to put the results of this study into context, the energy density calculations summarized in Fig. 11c and 11d are compared to other published studies that also consider the energetic impact of limiting substrate concentrations.

The number of Joules available to microorganisms per kg of fluid due to the disequilibrium created by the mixing of hydrothermal fluids and seawater can vary by

many orders of magnitude depending on the mixing ratio and the original compositions of the end-member fluids. This is clearly illustrated in a recent study in which the maximum amount of energy available from seawater mixing with fluids coming from 12 different hydrothermal systems has been calculated (Amend et al., 2011). In this study it is shown that reactions such as H_2S, CH_4 , H_2 and Fe(II) oxidation can provide more than 1000 J/kg H_2O while sulfate reduction, methanogenesis and the anaerobic oxidation of methane (AOM) can provide hundreds of J / kg H_2O. However, the amount that each reaction provides varies considerably from one system to the next depending on the types of rocks that the hydrothermal fluids circulate through. Other studies have shown similar results. For instance, hydrothermal fluids from ultramafic systems that mix with seawater can provide up to 3700 J /kg H_2O for H_2 oxidation (McCollom, 2007), but in fluid mixing from a basalt-hosted mid-ocean ridge system (East Pacific Rise, EPR, 21^o N OBS vent) only ~35 J/kg H_2O (Shock and Holland, 2004). Similarly, the ultramafic mixtures tend to supply much more energy per kg H_2O than other types of hydrothermal systems for methane oxidation (2100 J /kg H_2O) and Fe(II) oxidation (1300 J /kg H_2O) as compared to EPR fluids, 30-150 J /kg H_2O (McCollom and Shock, 1997). In an analysis of the energy available in a hydrothermal plume, the energy available from a similar set of chemolithoautotrophic reactions are more similar to the EPR fluids (McCollom, 2000).

In terms of sulfur-based metabolisms, ultramafic hydrothermal systems can provide up to 900 J / kg H_2O (S^0 oxidation and sulfate reduction) (McCollom, 2007) whereas the maximum amount of energy from sulfide oxidation at EPR-type systems can generate up to 3200 J /kg H_2O,but sulfate reduction only yields tens of J / kg H_2O (McCollom and Shock, 1997). A more recent assessment of fluids from EPR shows that

elemental sulfur oxidation and H_2S oxidation to sulfate and S^0 all provide ~ 30 J / kg H_2O, with S^0 and sulfate reduction below about 20 J / kg H_2O. The amount of energy available from S-based reactions at the 6 sites considered in this study are more similar to these latter values. It should be noted that typically, the most exergonic reactions for a particular ratio of hydrothermal fluids : seawater are the ones that are reported in the studies mentioned above. However, under unfavorable mixing ratios, the amount of energy available from these reactions is orders of magnitude lower than the most optimal conditions. This is clearly shown in the current study and one carried out by (Houghton and Seyfried Jr., 2010).

6. Concluding remarks

While subsurface processes associated with deep-sea hydrothermal vent fluids are fairly well understood, shallow-sea venting has received much less attention. It has been suggested that there is a definable link between subsurface hydrothermal processes and the associated microbial communities (Flores et al., 2011; Meyer-Dombard et al., 2011; Nakagawa et al., 2005; Nunoura and Takai, 2009; Price et al., 2013b). Shallow-sea vents provide excellent opportunities to investigate this link.

Evaluation of geochemistry from three shallow-sea vent sites located off shore Panarea Island indicate that, although trends were similar for pH, temperature, Mg, and SO_4, each site displayed distinct differences in major and trace element composition. As such, at least 3 end-member solutions are plausible, each of which mixes with ambient seawater upon discharge. Type 1 fluids, which discharge from “Hot Lake”, have the highest salinities, and seem to be direct discharge of the deepest part of the hydrothermal

reservoir underlying the island. Based on Cl/Br ratios, these fluids do not seem to have undergone phase separation, and are mostly influenced by water-rock reactions. Extreme salinities may result from long term distillation. Type 2 fluids, which are present as vent and gas-rich fluids from the Black Point and La Calcara sites, respectively, are lower in salinity relative to Type 1 fluids, yet higher salinity compared to seawater. These fluids seem to be derived from a shallower low-salinity reservoir, which may have lower salinity due to entrainment of seawater. This indicates that the Panarea system maintains a layered reservoir with double-diffusive circulation. Type 3 fluids, which are represented by pore fluids from Black Point and La Calcara, develop as a result of gas scrubbing as exsolved gases percolate through sediment pore fluids.

Thermodynamic calculations indicate that sulfur (H_2S and S^0) oxidation by O_2 should be the dominant metabolic activity at each site and fluid type investigated. Differences are primarily a function of the abundance of H_2S and S^0 as electron donors, and the O_2 provided, e.g., in Black Point pore fluids as a result of shallow, near-seafloor seawater entrainment. CH_4 oxidation is much more prevalent at the La Calcara site, and Mn^{2+} oxidation is likely at the Black Point site, reflecting elevated concentrations of these electron donors.

The combined approach of describing both subsurface hydrothermal processes and thermodynamic calculation of catabolic potential allows us to evaluate the related importance of both abiotic and biotic influences as agents of global element cycling. Future research on shallow-sea hydrothermal venting should focus more on the influence that abundant free gas discharge has on the evolution of hydrothermal vent fluid

chemistry, particularly its role in providing electron donors through gas scrubbing, and its role in providing electron acceptors (O_2) by seawater entrainment.

Acknowledgements

We thank two anonymous reviewers for their excellent insights into the subsurface processes occurring at Panarea. Funding for this research was provided by the MARUM Center for Marine Environmental Sciences. Additional support was provided by NSF-RIDGE grant 0937337 (to JPA) and the NSF-funded Center for Dark Energy Biosphere Investigations (C-DEBI) Postdoctoral Scholar Program (to DEL), and the Hydrothermal Vents Research Group in the MARUM Center for Environmental Sciences. LaRowe and Amend benefitted from financial assistance provided by the Center for Dark Energy Biosphere Investigations (C-DEBI) and the NASA Astrobiology Institute — Life Underground (NAI-LU). This is C-DEBI contribution X and NAI-LU contribution Y (to be assigned if accepted for publication). We additionally thank Wolfgang Bach, Anke Meyerdierks, Chia-I Huang, Florence Schubotz, Roger Summons, and Benjamin Brunner for helpful discussions. The manuscript also benefitted from discussions with the Univ. Leeds high-temperature group (and especially Jorgen Rosenqvist and Matthew Pankhurst). Logistical support on Panarea was provided by the Amphibia dive center and the staff at the Hotel Chincota.

References

Achterberg, E. et al., 2001. Determination of iron in seawater. Analytica Chimica Acta, 442: 1-14.

Akerman, N., Price, R., Pichler, T., Amend, J.P., 2011. Energy sources for chemlithotrophs in an arsenic- and iron-rich shallow-sea hydrothermal system. Geobiology, 9: 436-445.

Alt, J.C., 1994. A sulfur isotopic profile through the Troodos Ophiolite, Cyprus: Primary composition adn the effects of seawater hydrothermal alteration. Geochimica et Cosmochimica Acta, 58: 1825-1840.

Alt, J.C., 1995. Seafloor processes in mid-ocean ridge hydrothermal systems. In: Humphris, S.E., Zierenberg, R.A., Mullineaux, L.S., Thomson, R.E. (Eds.), Seafloor Hydrothermal Systems: Physical, Chemical, Biological, and Geological Interactions. American Geophysical Union, Washington, D.C., pp. 85-114.

Alt, J.C., Honnorez, J., Laverne, C., Emmermann, R., 1986. Hydrothermal alteration of a 1 km section through the upper oceanic crust, Deep Sea Drilling Project Hole 504B: Mineralogy, chemistry and evolution of seawater-basalt ineractions. Journal of Geophysical Research: Solid Earth, 91(B10): 10309-10335.

Amend, J., McCollom, T., Hentscher, M., Bach, W., 2011. Catabolic and anabolic energy for chemolithoautotrophs in deep-sea hydrothermal systems hosted in different rock types. Geochimica et Cosmochimica Acta, 75: 5736-5748.

Amend, J.P., Meyer-Dombard, D.R., Sheth, S.N., Zolotova, N., Amend, A.C., 2003a. Palaeococcus helgesonii sp. nov., a facultatively anaerobic, hyperthermophilic archaeon from a geothermal well on Vulcano Island, Italy. Archives of Microbiology, 179: 394-401.

Amend, J.P., Rogers, K.L., Shock, E.L., Gurrieri, S., Inguaggiato, S., 2003b. Energetics of chemolithoautotrophy in the hydrothermal system of Vulcano Island, southern Italy. Geobiology, 1: 37-58.

Amend, J.P., Shock, E.L., 2001. Energetics of overall metabolic reactions of thermophilic and hyperthermophilic Archaea and Bacteria. FEMS Microbiol. Rev., 25(2): 175 - 243.

Becke, R., Merkel, B., Pohl, T., 2009. Mineralogical and geological characteristics of the shallow-water massive sulfide precipitates of Panarea, Aeolian Islands, Italy. In: Merkel, B., Schipek, M. (Editors), Research in shallow marine and fresh water systems. Freiberg Online Geology, TU Bergakademie Freiberg, pp. 94-100.

Berg, J., 2011. Microbial characterization of white mats in a hydrothermally-influenced, sulfur-rich brine pool. Senior Honors Thesis Thesis, Washington University in St. Louis, St. Louis.

Berndt, M.E., 1987. Experimental and theoretical constraints on the origin of mid-ocean ridge geothermal fluids, University of Minnesota, Minneapolis, Minnesota.

Berndt, M.E., Person, M.E., Seyfried, W.E., 2001. Phase separation and two-phase flow in seafloor hydrothermal systems, 11th Annual V. M. Goldschmidt Conference. Geochemical Society, Hot Springs, VA.

Berndt, M.E., Seyfried, W.E., 1993. Calcium and sodium exchange during hydrothermal alteration of calcic plagioclase at 400 C adn 400 bars. Geochimica et Cosmochimica Acta, 57(18): 4445-4451.

Berndt, M.E., Seyfried, W.E., Beck, J.W., 1988. Hydrothermal alteration processes at midocean ridges: experimental and theoretical constraints from Ca and Sr exchange reactions and Sr isotopic ratios. Journal of Geophysical Research, 93(B5): 4573-4583.

Berndt, M.E., Seyfried, W.E., Janecky, D.R., 1989. Plagioclase and epidote buffering of cation ratios in mid-ocean ridge hydrothermal fluids - experimental results in and near the supercritical region. Geochimica et Cosmochimica Acta, 53(9): 2283-2300.

Bischoff, J.L., Disckson, F.W., 1975. Seawater-basalt interaction at 200 °C and 500 bars: implications for origin of sea-floor heavy-metal deposits and regulation of seawater chemmistry. Earth and Planetary Science Letters, 25: 385-397.

Bischoff, J.L., Rosenbauer, R.J., 1985. An empirical equation of state for hydrothermal seawater (3.2 percent NaCl). American Journal of Science, 285: 725-763.

Bischoff, J.L., Rosenbauer, R.J., 1987. Phase separation in seafloor geothermal systems: An experimental study of the effects on metal transport. American Journal of Science, 287: 953-978.

Bischoff, J.L., Rosenbauer, R.J., 1989. Salinity variations in submarine hydrothermal systems by layered double-diffusive convection. Journal of Geology, 97(5): 613-623.

Butterfield, D.A., Massoth, G.J., 1994. Geochemistry of north Cleft segment vent fluids: Temporal changes in chlorinity and their possible relation to recent volcanism. Journal of Geophysical Research, 99(B3): 4951-4968.

Butterfield, D.A., Massoth, G.J., McDuff, R.E., Lupton, J.E., Lilley, M.D., 1990. Geochemistry of hydrothermal fluids from Axial Seamount hydrothermal vent field, Juan de Fuca Ridge: subseafloor boiling and subsequent fluid-rock interaction. Journal of Geophysical Research, 95: 12895-12921.

Calanchi, N. et al., 2002. Petrology and geochemistry of volcanic rocks from the island of Panarea: implications for mantle evolution beneath the Aeolian island arc (southern Tyrrhenian sea). Journal of Volcanology and Geothermal Research, 115: 367-395.

Calanchi, N., Tranne, C.A., Lucchini, F., Rossi, P.L., Villa, I.M., 1999. Explanatory notes to the geologic map (1:10,000) of Panarea and Basiluzzo islands (Aeolian arc. Italy). Acta Vulcanologica, 11(2): 223-243.

Caracausi, A. et al., 2005. Changes in fluid geochemistry and physico-chemical conditions of geothermal systems caused by magmatic input: The recent abrupt outgassing off the island of Panarea (Aeolian Islands, Italy). Geochimica et Cosmochimica Acta, 69(12): 3045-3059.

Charlou, J., Donval, J., Fouquet, Y., Jean-Baptiste, P., Holm, N., 2002. Geochemistry of high H2 adn CH4 vent fluids issuing from ultramafic rocks at the Rainbow hydrothermal field (36°14'N, MAR). Chemical Geology, 191: 345-359.

Cline, J., 1969. Spectrophotometric determination of hydrogen sulfide in natural waters. Limnology and Oceanography, 14(3): 454-458.

Craig, H., Lupton, J., 1981. Helium-3 and mantle volatiles in the ocean and oceanic crust. In: Emiliani, C.E. (Ed.), The Sea, v. 7, The Oceanic Lithosphere. Wiley, New York, pp. 391-428.

Dando, P.R., Aliani, S., others, a., 2000. Hydrothermal studies in the Aegean Sea. Phys. Chem. Earth, 25: 1-8.

Dando, P.R. et al., 1995. Gas venting rates from the submarine hydrothermal areas around the island of Milos, Hellenic volcanic arc. Continental Shelf Research, 15(8): 913-929.

Dando, P.R., Stüben, D., Varnavas, S.P., 1999. Hydrothermalism in the Mediterranean Sea. Progress in Oceanography, 44(1-3): 333-367.

De Astis, G., Peccerillo, A., Kempton, P., La Volpe, L., Wu, T.W., 2000. Transition from calc-alkaline to potassium-rich magmatism in subduction environments: geochemical and Sr, Nd, Pb isotopic constraints from the Island of Volcano (Aeolian arc). Contrib. Miner. Petrol., 139: 684-703.

Dekov, V.M., Kamenov, G.D., Abrasheva, M.D., Capaccioni, B., Munnik, F., 2013. Mineralogical and geochemical investigation of seafloor massive sulfides from Panarea Platform (Aeolian Arc, Tyrrhenian Sea). Chemical Geology, 335: 136-148.

Delalande, M. et al., 2011. Fluid geochemistry of natural manifestations from the Southern Poroto-Rungwe hydrothermal system (Tanzania): Preliminary conceptual model. Journal of Volcanology and Geothermal Research, 199: 127-141.

Edmonds, H., Edmonds, J.M., 1995. A three-component mixing model for ridge-crest hydrothermal fluids. Earth and Planetary Science Letters, 14: 53-67.

Ellam, R.H., Hawkesworth, C.J., Menzies, M.A., Rogers, N.W., 1989. The volcanism of Southern Italy: Role of subduction and relationship between potassic and sodic alkaline magmatism. Journal of Geophysical Research, 94: 4589-4601.

Felbeck, H., Somero, G.N., 1982. Primary production in deep-sea hydrothermal vent organisms: roles of sulfide-oxidizing bacteria. Trends in Biochemical Sciences, 7(6): 201-204.

Fitzsimons, M.F. et al., 1997. Submarine hydrothermal brine seeps off Milos, Greece: Observations and geochemistry. Marine Chemistry, 57: 325-340.

Flores, G.E. et al., 2011. Microbial community structure of hydrothermal deposits from geochemically different vent fields along the Mid-Atlantic Ridge. Environmental Microbiology, 13(8): 2158-2171.

Fournier, R.O., 2007. Hydrothermal systems and volcano geochemistry. In: D, D. (Ed.), Volcano Deformation. Praxis Publishing Ltd., Chichester, UK, pp. 323-341.

Foustoukos, D.I., Houghton, J.L., Seyfried, W.E., Sievert, S.M., Cody, G.D., 2011. Kinetics of H2-O2-H2O redox equilibria and formation of metastable H2O2 under low temperature hydrothermal conditions. Geochimica et Cosmochimica Acta, 75: 1594-1607.

Foustoukos, D.I., Seyfried, W.E., 2007. Fluid phase separation processes in submarine hydrothermal systems. Reviews in Mineralogy and Geochemistry, 65: 213-239.

Francalanci, L., Taylor, S.R., McCulloch, M.T., Woodhead, J., 1993. Geochemical and isotopic variations in the calc-alkaline rocks of the Aeolian Arc (Southern Italy): constraints on the magma genesis. Contrib. Miner. Petrol., 113: 300-313.

Gallant, R.M., Von Damm, K.L., 2006. Geochemical controls on hydrothermal fluids from the Kairei and Edmond vent fields, 23° - 25° S, Central Indial Ridge. Geochemistry, Geophysics, Geosystems, 7(6): 1-24.

Gamo, T. et al., 1997. Acidic and sulfate-rich hydrothermal fluids from the Manus back-arc basin, Papua New Guinea. Geology, 25(2): 139-142.
German, C.R., Von Damm, K.L., 2003. Hydrothermal Processes. In: Holland, H.D., Turekian, K.K. (Eds.), Treatise on Geochemistry. Elsevier, pp. 145-180.
Grasshoff, K., Ehrhardt, M., Kremling, K., 1983. Methods of seawater analysis. Verlag Chemie, Weinheim.
Gugliandolo, C., Italiano, F., Maugeri, T.L., 2006. The submarine hydrothermal system of Panarea (Southern Italy): biogeochemical processes at the thermal fluids-sea bottom interface. Annals of Geophysics, 49(2/3): 783-792.
Gugliandolo, C. et al., 1999. Submarine hydrothermal vents of the Aeolian Islands: Relationship between microbial communities and thermal fluids. Geomicrobiology Journal, 16(1): 105-117.
Gunnarsson, I., Arnorsson, S., 2000. Amorphous silica solubility and the thermodynamic properties of H_3SiO_4 in the range of 0° to 350° at Psat. Geochimica et Cosmochimica Acta, 64(13): 2295-2307.
Haeckel, M., Boudreau, B.P., Wallmann, K., 2007. Bubble-induced porewater mixing: A 3-D model for deep porewater irrigation. Geochimica et Cosmochimica Acta, 71: 5135-5154.
Hannington, M., De Ronde, C.E.J., Petersen, S., 2005. Sea-floor tectonics and submarine hydrothermal systems. Economic Geology, 100th Anniversary Volume: 111-141.
Haymon, R.M., 1983. Growth history of hydrothermal black smoker chimneys. Nature, 301: 695-698.
Hedenquist, J.W., Lowenstern, J.B., 1994. The role of magmas in the formation of hydrothermal ore deposits. Nature, 370: 519-527.
Heinrich, C.A., Driesner, T., Stefánsson, A., Seward, T.M., 2004. Magmatic vapor contraction and the transport of gold from the porphyry environment to epithermal ore deposits. Geology, 32(9): 761-764.
Helgeson, H.C., 1969. Thermodynamics of hydrothermal systems at elevated temperatures and pressures. Amer. J. Sci., 267: 729-804.
Helgeson, H.C., Kirkham, D.H., Flowers, G.C., 1981. Theoretical prediction of thermodynamic behavior of aqueous electrolytes at high pressures and temperatures: 4. Calculation of activity coefficients, osmotic coefficients, and apparent molal and standard and relative partial molal properties to 600^{o}C and 5 kb. Amer. J. Sci., 281(10): 1249 - 1516.
Henley, R.W., Ellis, A.J., 1983. Geothermal systems anchient and modern: A geochemical review. Earth-Science Reviews, 19: 1-50.
Hernandez-Sanchez, M.T. et al., 2014. Further insights into how sediment redox status controls the preservation and composition of sedimentary organic biomarkers. Organic Geochemistry, 76: 220-234.
Houghton, J.L., Seyfried Jr., W.E., 2010. An experimental and theoretical approach to determing linkages between geochemical variability and microbial biodiversity in seafloor hydrothermal chimneys. Geobiology, 8: 457-470.
Huang, C.I., 2012. Molecular Ecology of Free-Living Chemoautotrophic Microbial Communities at a Shallow-sea Hydrothermal Vent, University of Bremen, Bremen, Germany.

Imhoff, I., Hügler, M., 2009. Life at deep sea hydrothermal vents - Oases under water. The International Journal of Marine and Coastal Law, 24(2): 201-208.
Inskeep, W. et al., 2005. On the energetics of chemolithotrophy in nonequilibrium systems: case studies of geothermal springs in Yellowstone National Park. Geobiology, 3: 297-317.
Inskeep, W.P., McDermott, T.R., 2005. Geomicrobiology of acid–sulfate–chloride springs in Yellowstone National Park. In: Inskeep, W.P., McDermott, T.R. (Eds.), Geothermal Biology and Geochemistry in Yellowstone National Park. Thermal Biology Institute, Montanta State University, pp. 143-162.
Ishibashi, J., 1995. Geochemistry of phase-separated hydrothermal fluids of the North Fiji Basin, Southwest Pacific. In: Sakai, H., Nozaki, Y. (Eds.), Biogeochemical Processes and Ocean Flux in the Western Pacific. Terrapub, Tokyo, pp. 453-467.
Italiano, F., Nuccio, F., 1991. Geochemical investigations of submarine volcanic exhalations to the east of Panarea, Aeolian Islands, Italy. Journal of Volcanology and Geothermal Research, 46: 125-141.
Johnson, J.W., Oelkers, E.H., Helgeson, H.C., 1992. SUPCRT92 - A software package for calculating the standard molal thermodynamic properties of minerals, gases, aqueous species, and reactions from 1 bar to 5000 bar and 0^{o}C to 1000^{o}C. Comput. Geosci., 18(7): 899 - 947.
Kenig, E., Górak, A., 2005. Reactive Absorption. In: Sundmacher, K., Seidel-Morgenstern (Eds.), Integrated Chemical Processes: Synthesis, Operation, Analysis and Control. John Wiley & Sons.
Klinkhammer, G., Rona, P., Greaves, M., Elderfield, H., 1985. Hydrothermal manganese plumes in the Mid-Atlantic Ridge rift valley. Nature, 314: 727-731.
Lan, C.-R., Alfassi, Z.B., 1994. Direct determination of manganese in seawater by electrothermal atomic absorption spectrometry with sodium hydroxide as chemical modifier for interference removal. Analyst, 119: 1033-1035.
LaRowe, D.E., Amend, J.P., 2014. Energetic constraints on life in marine deep sediments. In: Kallmeyer, J., Wagner, K. (Eds.), Life in Extreme Environments: Microbial Life in the Deep Biosphere. De Gruyter, pp. 279-302.
LaRowe, D.E., Dale, A.W., Regnier, P., 2008. A thermodynamic analysis of the anaerobic oxidation of methane in marine sediments. Geobiology, 6: 436-449.
LaRowe, D.E., Van Cappellen, P., 2011. Degradation of natural organic matter: A thermodynamic analysis. Geochim. Cosmochim. Acta, 75: 2030-2042.
Lowell, J.D., Guilbert, J.M., 1970. Lateral and vertical alteration-mineralization zoning in porphyry ore deposits. Economic Geology, 65: 373-408.
Lupton, J. et al., 2008. Venting of a separate CO2-rich gas phase from submarine arc volcanoes: Examples from the Mariana and Tonga-Kermadec arcs. Journal of Geophysical Research, 113: 1-21.
Luther, G.W., Tsamakis, E., 1989. Concentration and form of dissolved sulfide in the oxic water column of the ocean. Marine Chemistry, 27(3-4): 165-177.
Lutz, R.A., Kennish, M., 1993. Ecology of deep-sea hydrothermal vent communities: A review. Reviews of Geophysics, 31(3): 211-242.
Martin, J.B., 1999. Nonconservative behavior of Br/Cl ratios during alteration of volcaniclastic sediments. Geochimica et Cosmochimica Acta, 63: 383-391.

Martin, J.B., Gieskes, J.M., Torres, M., Kastner, M., 1993. Bromine and iodine in Peru margin sediements adn pore fluids: Implications for fluid origins. Geochimica et Cosmochimica Acta, 57(18): 4377-4389.

Maugeri, T.L. et al., 2009. Bacterial and archaeal populations at two shallow hydrothermal vents off Panarea Island (Eolian Islands, Italy). Extremophiles, 13: 199-212.

McArthur, J.M., Donovan, D.T., Thirlwall, M.F., Fouke, B.W., Mattey, D., 2000. Strontium isotope profile of the early Toarcian (Jurassic) oceanic anoxic event, the duration of ammionite biozones, and belemnite palaeotemperatures. Earth and Planetary Science Letters, 179: 269-285.

McCollom, T.M., 2000. Geochemical constraints on primary productivity in submarine hydrothermal vent plumes. Deep-Sea Res. Part I - Oceanogr. Res. Pap., 47(1): 85-101.

McCollom, T.M., 2007. Geochemical constraints on sources of metabolic energy for chemolithoautotrophy in ultramafic-hosted deep-sea hydrothermal systems. Astrobiology, 7: 933-950.

McCollom, T.M., Shock, E.L., 1997. Geochemical constraints on chemolithoautotrophic metabolism by microorganisms in seafloor hydrothermal systems. Geochim. Cosmochim. Acta, 61(20): 4375 - 4391.

Meyer-Dombard, D.R., Price, R.E., Pichler, T., Amend, J.P., 2011. Prokaryotic populations in arsenic-rich shallow-sea hydrothermal sediments of Ambitle Island, Papua New Guinea. Geomicrobiology Journal (in press).

Moest, R., 1975. Hydrogen sulfide determination by the methylene blue method. Analytical Chemistry, 47(7): 1204-1205.

Mottl, M.J., 1983. Metabasalts, axial hot springs, and the structure of hydrothermal systems at mid-ocean ridges. Geological Society of America Bulletin, 94: 161-180.

Mottl, M.J., Corr, R.F., Holland, H.D., 1974. Chemical exchange between seawater and mid-ocean ridge basalt during hydrohtemral alteration: an experimental study, GSA annual meeting.

Müller, C., 2011. Geothermal state of shallow submarine geothermal systems and isotopic signatures of Panarea, Aeolian Islands (Italy), Technische Universität Bergakademie Freiberg, Freiberg, Germany, 141 pp.

Nakagawa, S. et al., 2005. Variability in microbial community and venting chemistry in a sediment-hosted backarc hydrothermal system: Impacts of subseafloor phase-separation. FEMS Microbiological Ecology, 54: 141-155.

Nehlig, P., 1993. Interactions between magma chambers and hydrothermal systems: oceanic and ophiolitic constraints. Journal of Geophysical Research, 98(19): 621-633.

Neri, G., Barberi, G., Orecchio, B., Aloisi, M., 2002. Seismotomography of the crust in the transition zone between the southern Tyrrhenian and Sicilian tectonic domains. Geophysical Research Letters, 29(23): 50-1 - 50-4.

Nunoura, T., Takai, K., 2009. Comparison of microbial communities associated with phase-separation-induced hydrothermal fluids at the Yonaguni Knoll IV hydrothermal field, the Southern Okinawa Trough. FEMS Microbial Ecology, 67: 351-370.

Oosting, S.E., Von Damm, K.L., 1996. Bromide/chloride fractionation in seafloor hydrothermal fluids from 9-10ºN East Pacific Rise. Earth and Planetary Science Letters, 144: 133-145.

Osburn, G.R., LaRowe, D.E., Momper, L., Amend, J.P., 2014. Chemolithotrophy in the continental deep subsurface: Sanford Underground Research Facility (SURF), USA. Front. Microbiol., 5: Article 610.

Peccerillo, A., 2001. Geochemical similarities between Vesuvius, Phlegraean Fields and Stromboli volcanoes: petrogenetic, geodynamic and volcanological implications. Miner. Petrol., 73: 93-105.

Peccerillo, A., Panza, G., 1999. Upper mantle domains beneath central-southern Italy: petrological, geochemical and geophysical constraints. Pure Appl. Geophys., 156: 421-443.

Peters, M., Strauss, H., Peterson, S., Kummer, N.-A., Tomazo, C., 2011. Hydrothermalism in the Tyrrhenian Sea: Inorganic and microbial sulfur cycling as revealed by geochemical and multiple sulfur isotope data. Chemical Geology, 280: 217-231.

Petersen, S. et al., 2007. Drilling submarine hydrothermal sites in the Tyrrhenian Sea, Italy, during Meteor cruise M73/2, University of Hamburg Institute of Oceanography.

Pichler, T., 2005. Stable and radiogenic isotopes as tracers for the origin, mixing and subsurface history of fluids in submarine shallow-water hydrothermal systems. Journal of Volcanology and Geothermal Research, 139: 211-226.

Pichler, T. et al., 2006. A natural laboratory to study arsenic geobiocomplexity. EOS, 87: 221-225.

Pichler, T., Veizer, J., Hall, G.E.M., 1999. The chemical composition of shallow-water hydrothermal fluids in Tutum Bay, Ambitle Island, Papua New Guinea and their effect on ambient seawater. Marine Chemistry, 64: 229-252.

Pirajno, F., 2009. Hydrothermal processes and mineral systems, 1. Springer, 1250 pp.

Prautsch, A., Stanulla, R., Pohl, T., Merkel, B., 2013. Geochemical-mineralogical investigation of degassing structures caused by recent volcanic hydrothermalism - Case study: La Calcara, Isle of Panarea (Italy). In: Pichler, T., Häusler, S., Tsounis, G. (Editors), Research in Shallow Marine and Fresh Water Systems, 3rd International Workshop. MARUM, Bremen, Germany, pp. 41-44.

Price, R.E. et al., 2013a. Archaeal and bacterial diversity in an arsenic-rich shallow-sea hydrothermal system undergoing phase separation. Frontiers in Extreme Microbiology, 4: Article 158.

Price, R.E., Pichler, T., 2005. Distribution, speciation and bioavailability of arsenic in a shallow-water submarine hydrothermal system, Tutum Bay, Ambitle Island, PNG. Chemical Geology, 224: 122-135.

Price, R.E. et al., 2012. Processes influencing extreme As enrichment in shallow-sea hydrothermal fluids of Milos Island, Greece. Chemical Geology, in press.

Price, R.E. et al., 2013b. Processes influencing extreme As enrichment in shallow-sea hydrothermal fluids of Milos Island, Greece. Chemical Geology, 348: 15-26.

Reeves, E.P. et al., 2011. Geochemistry of hydrothermal fluids from the PACMANUS, Northeast Paul and Vienna Woods hydrothermal fields, Manus Basin, Papua New Guinea. Geochimica et Cosmochimica Acta, 75(4): 1088-1123.

Resing, J.A. et al., 2007. Venting of acid-sulfate fluids in a high-sulfidation setting at NW Rota-1 submarine volcano on the Mariana Arc. Economic Geology, 102: 1047-1061.

Rogers, K.L., Amend, J.P., 2005. Archaeal diversity and geochemical energy yields in a geothermal well on Vulcano Island, Italy. Geobiology, 3: 319-332.

Rogers, K.L., Amend, J.P., 2006. Energetics of potential heterotrophic metabolisms in the marine hydrothermal system of Vulcano Island, Italy. Geochim. Cosmochim. Acta, 70: 610-6200.

Rogers, K.L., Amend, J.P., Gurrieri, S., 2007. Temporal changes in fluid chemistry and energy profiles in the Vulcano island hydrothermal system. Astrobiology, 7: 905-932.

Rouwet, D., Tassi, F., 2011. Geochemical monitoring of volcanic lakes. A generalized box model for active crater lakes. Annals of Geophysics, 54: 161-173.

Schroedinger, E., 1944. What is Life? Cambridge University Press, 194 pp.

Schulte, M.D., Shock, E.L., Wood, R., 2001. The temperature dependence of the standard-state thermodynamic properties of aqueous nonelectrolytes. Geochim. Cosmochim. Acta, 65(21): 3919 - 3930.

Seeberg-Elverfeldt, J., Schlüter, M., Feseker, T., Kölling, M., 2005. Rhizon sampling of pore waters near the sediment/water interface of aquatic systems. Limnology and Oceanography: Methods, 3: 361-371.

Seyfried, W.E., Berndt, M.E., Seewald, J.S., 1988. Hydrothermal alteration processes at mid-ocean ridges: Constraints from diabase alteration experiments, hot-spring fluids, and composition of the oceanic crust. Canadian Mineralogist, 26: 787-804.

Seyfried, W.E., Ding, K., Berndt, M.E., 1991. Phase equilibria constraints on the chemistry of hot spring fluids at mid-ocean ridges. Geochimica et Cosmochimica Acta, 55: 3559-3580.

Seyfried, W.E., Mottl, M.J., 1982. Hydrothermal alteration of basalt by seawater under seawater dominated conditions. Geochimica et Cosmochimica Acta, 46: 985-1002.

Seyfried, W.E., Seewald, J.S., Berndt, M.E., Ding, K., Foustoukos, D.I., 2003. Chemistry of hydrothermal vent fluids from the Main Endeavour Field, northern Juan de Fuca Ridge: Geochemical controls in the aftermath of the June 1999 seismic events. Journal of Geophysical Research, 108(B9): 2429.

Shanks III, W.C., 2012. Hydrothermal alteration in volcanogenic massive sulfide occurrence model.

Shock, E.L., Helgeson, H.C., 1988. Calculation of the thermodynamic and transport properties of aqueous species at high pressures and temperatures - Correlation algorithms for ionic species and equation of state predictions to 5 kb and 1000^{o}C. Geochim. Cosmochim. Acta, 52(8): 2009 - 2036.

Shock, E.L., Helgeson, H.C., 1990. Calculation of the thermodynamic and transport properties of aqueous species at high pressures and temperatures - Standard partial molal properties of organic species. Geochim. Cosmochim. Acta, 54(4): 915 - 945.

Shock, E.L., Helgeson, H.C., Sverjensky, D., 1989. Calculation of the thermodynamic and transport properties of aqueous species at high pressures and temperatures -

Standard partial molal properties of inorganic neutral species. Geochim. Cosmochim. Acta, 53(9): 2157 - 2183.

Shock, E.L., Holland, M., Meyer-Dombard, D., Amend, J.P., 2005. Geochemical sources of energy for microbial metabolism in hydrothermal ecosystems: Obsidian Pool, Yellowstone National Park, USA In: Inskeep, W.P., McDermott, T.R. (Eds.), Geothermal Biology and Geochemistry in Yellowstone National Park Thermal Biology Institute. Montana State University, pp. 95-112.

Shock, E.L. et al., 2010. Quantifying inorganic sources of geochemical energy in hydrothermal ecosystems, Yellowstone National Park, USA. Geochimica Cosmochimica Acta, 74: 4005-4043.

Shock, E.L., Holland, M.E., 2004. Geochemical energy sources that support the subseafloor biosphere. The subseafloor biosphere at mid-ocean ridges. In: Wilcock, W.S.D., DeLong, E.F., Kelley, D.S., Baross, J.A., Cary, S.C. (Eds.), Geophysical Monograph 144. American Geophysical Union, pp. 153–165.

Shock, E.L., McCollom, T.M., Schulte, M.D., 1995. Geochemical constraints on chemolithoautotrophic reactions in hydrothermal systems. Orig. Life Evol. Bios., 25(1-3): 141 - 159.

Shock, E.L., Oelkers, E., Johnson, J.W., Sverjensky, D., Helgeson, H.C., 1992. Calculation of the thermodynamic properties of aqueous species at high pressures and temperatures - Effective electrostatic radii, dissociation constants adn standard partial molal properties to 1000C adn 5 kbar. J. Chem. Soc. Faraday Trans., 88: 803-826.

Sieland, R., 2009. Chemical and isotopic investigations of submarine hydrothermal fluid discharges from Panarea, Aeolian Islands, Italy, Technische Universität Bergakademie Freiberg, Freiberg, Germany, 180 pp.

Spear, J.R., Walker, J.J., McCollom, T.M., Pace, N.R., 2005. Hydrogen and bioenergetics in the Yellowstone geothermal ecosystem. PNAS of the USA, 102(7): 2555-2560.

Sverjensky, D., Shock, E.L., Helgeson, H.C., 1997. Prediction of the thermodynamic properties of aqueous metal complexes to 1000^{o}C and 5 kb. Geochim. Cosmochim. Acta, 61(7): 1359 - 1412.

Tanger, J.C., Helgeson, H.C., 1988. Calculation of the thermodynamic and transport properties of aqueous species at high pressures and temperatures - Revised equations of state for the standard partial molal properties of ions and electrolytes. Amer. J. Sci., 288(1): 19 - 98.

Tarasov, V.G., Gebruk, A.V., Mironov, A.N., Moskalev, L.I., 2005. Deep-sea and shallow-water hydrothermal vent communities: Two different phenomena? Chemical Geology, 224: 5-39.

Tassi, F. et al., 2009. Low-pH waters discharging from submarine vents at Panarea Island (Aeolian Islands, southern Italy) after the 2002 gas blast: Origin of hydrothermal fluids and implications for volcanic surveillance. Applied Geochemistry, 24: 246-254.

Teske, A.P., Callaghan, A.V., LaRowe, D.E., 2014. Biosphere Frontiers of subsurface life in the sedimented hydrothermal system of Guaymas Basin. Front. Microbiol., 5: 1-11.

Tivey, M.K., 2007. Generation of seafloor hydrothermal vent fluids and associated mineral deposits. Oceanography, 20(1): 50-65.

Vick, T.J., Dodsworth, J.A., Costa, K.C., Shock, E.L., Hedlund, B.P., 2010. Microbiology and geochemistry of Little Hot Creek, a hot spring environment in the Long Valley Caldera. Geobiology, 8: 140-154.

Von Damm, K.L., 2000. Chemistry of hydrothermal vent fluids from 9 -10 N, Ease Pacific Rise; "time zero," the immediate posteruptive period. Journal of Geophysical Research, 105: 11203-11222.

Von Damm, K.L. et al., 2003. Extraordinary phase separation and segregation in vent fluids from the southern East Pacific Rise. Earth and Planetary Science Letters, 206: 365-378.

Windman, T., 2010. Organic Compounds in Hydrothermal Systems. , Arizona State University, Tempe, Arizona, USA.

Wolery, T.J., Sleep, N.H., 1976. Hydrothermal circulation and geochemical flux at mid-ocean ridges. The Journal of Geology, 84(3): 249-275.

Yang, K., Scott, S.D., 1996. Possible contribution of a metal-rich magmatic fluid to a sea-floor hydrothermal system. Nature, 383(6599): 420-423.

Figure Captions:

Fig. 1. (a) Location of the island of Panarea and the submarine hydrothermal vents selected for this investigation. Sampling sites are indicated in (b) for La Calcara, Hot Lake and Black Point.

Fig. 2. (a-left) Underwater photographs of the Hot Lake area. Depression in the surrounding rocks is approximately 4 m by 6 m, and is filled with hydrothermal brine (see diver for scale). (a-right) close-up of microbial filaments in Hot Lake. (b-left) General area around Black Point (see diver for scale) and (b-right) close-up of white smoker and 'chimney'. (c-left) General area picture of La Calcara (see diver for scale) and (c-right) close-up of 135 °C gas-rich vents where anhydrite precipitation occurs.

Fig. 3. Measured field geochemistry data for Panarea fluids, (a) temperature versus pH. (b) temperature versus H_2S, and (c) H_2S versus pH. Note that Black Point vent and La Calcara gas-rich fluids often have the most extreme values, although Hot Lake fluids have the highest H_2S concentrations. Symbols in 3a are the same for 3b and 3c.

Fig. 4. Two-phase curve for seawater, including the critical point (c.p.) of seawater (c.p.= 407 °C, 298 bars), and the maximum vent temperatures for hydrothermal systems in different volcanic and tectonic settings (data from Hannington et al., 2005; curve from Bischoff and Rosenbauer, 1987; c.p. from Bischoff and Rosenbauer, 1984). Note slope of curve shallows significantly at >200 m, indicating that changes in pressure will dominate over changes in temperature. Grey area in upper left designates the pressure and temperature conditions encountered in shallow-sea hydrothermal vent systems.

Fig. 5. Hypothetical model of subsurface processes occurring in many hydrothermal systems. See text for details. (a) Low temperature water-rock reactions, (b) high temperature water-rock reactions, (c) magmatic volatile inputs, (d) phase separation, (e) continued water-rock reactions, and (f) degassing of dissolved volatiles. Note: 1) Panarea Type 1 fluids are directly fed by deep recirculating brine reservoir and form a brine pool due to extremely high salinity, 2) Type 2 fluids are focused upflow from the shallower brine which has been diluted by seawater, and 3) Type 3 fluids are derived from volatile degassing at lower pressures, followed by gas scrubbing to seawater-like pore fluids.

Fig. 6. (a) Measured concentrations of Mg^{2+} vs. SO_4^{2-} for Panarea fluids, with two possible projected intercepts. Horizontal and vertical lines in (a) indicate equivalent seawater concentrations. (b), Mg^{2+} vs. K (c) and Mg^{2+} vs. Na (c) for all hydrothermal fluids analyzed in this study. Note "triple-trend" mixing, and designation of Type 1, Type 2, and Type 3 fluids in (b) and (c). Starred data points indicate samples used in bioenergetics calculations, (b) and (c) include data previously collected by the National Institute of Geophysics and Volcanology (INGV, as noted) and confirms different mixing trends for Type 1, Type 2, and Type 3 fluids. (d) Mg vs. Ca, (e) Mg vs. Sr, (f) Mg vs. B, (g) Mg vs. Cl, and (h) Mg vs Br. Triple trends and 3 fluid types are present but not marked in (d) through (h). Symbols in 6a the same for other plots.

Fig. 7. End-member plots for Cl vs. Na (a), Cl vs Ca (b) concentrations, and end-member element rations for Na/Cl vs. Ca/Cl (c), and Na/Cl vs. Sr/Cl (d). (e) shows $^{87}Sr/^{86}Sr$ isotopic ratios for selected vent fluids from this study, plotted along with ratios for surrounding rock samples (Ash layer and * from Calanchi et al. (2002); ** from INGV database). Data trend towards subsurface rocks with a "Stromboli affinity". (note: the precision and accuracy of the data used for the mixing end-members is much smaller than the size of the symbols used, and so even the most conservative deviations from the considered mixing end-member are largely ignorable as they will bear no impact on the discussion or have minimal, if any, impact on the calculations). Symbols in 7a the same for 7b-7d. MOR = mid-ocean ridge systems; R-HS = ridge – hot spot intersections; Sed. = sedimented; IBABs = intraoceanic back-arc basins; IHS = intraplate hot spot; UM = ultramafic; Arc – BAB = transitional arc and back-arc. Other vent data from Hannington et al. (2005).

Fig. 8. Data plots used for evaluation of phase separation. Measured Cl vs. Na (a) Cl vs. Br (b), and Cl vs. Br/Cl (c) for hydrothermal fluids from each location. End-member Cl vs. Br/Cl (d) and (c) Cl vs. B/Cl (e) for Panarea hydrothermal fluids analyzed in this study. Symbols in 8a the same for other plots.

Fig. 9. (a) SEM image of hydrothermal precipitates occurring at the sediment / water interface where ~135 °C gas-rich fluids discharge at La Calcara. EDX analysis results, indicating the precipitates are anhydrite ($CaSO_4$), are shown upper right. (b) Ca vs. SO4 plot indicating removal of these elements in pore fluids, and (c) anhydrite solubility (□), as a function of temperature using seawater as the starting fluid.

Fig. 10. Trace element plots: (a) Mg vs. Mn, (b) Mg vs Ba, (c) Mg vs Li, (d) Mg vs Rb, (e) Mg vs. Cs, (f) Mg vs Si, and (g) Mg vs. Fe concentrations for the Panarea hydrothermal fluids. Symbols in 10a the same for other plots.

Fig. 11. Gibbs energies, ΔG_r, of the 61 catabolic reactions listed in Table 1 per mole of electron transferred colored by (a) oxidant and (b) electron donor (ED). (c) and (d) represent energy per kilogram of H_2O colored by oxidant and electron donor, respectively. The temperatures and compositions used to calculate these values are those describing the six samples locations summarized in Table 3. The horizontal bars in each panel denote the range of Gibbs energies for the indicated reaction for all sample locations. The colors of the bars refer to the types of electron acceptors and donors in each of the reactions, respectively.

Fig. 12. Comparison of energy available on a per site basis after removal of Reactions 43 and 44, the oxidation of NH_4^+ by MnO_2.

Fig. 1.

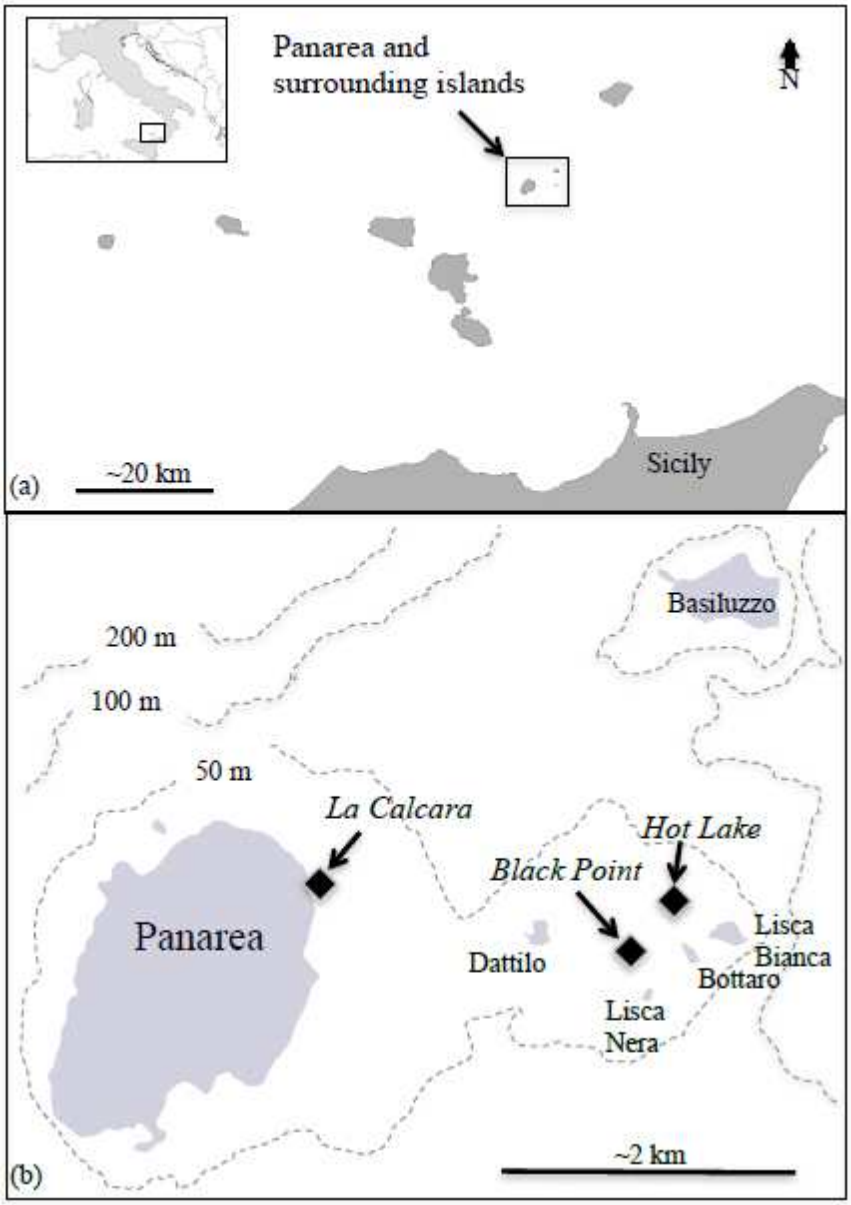

Fig. 2.

Fig. 3.

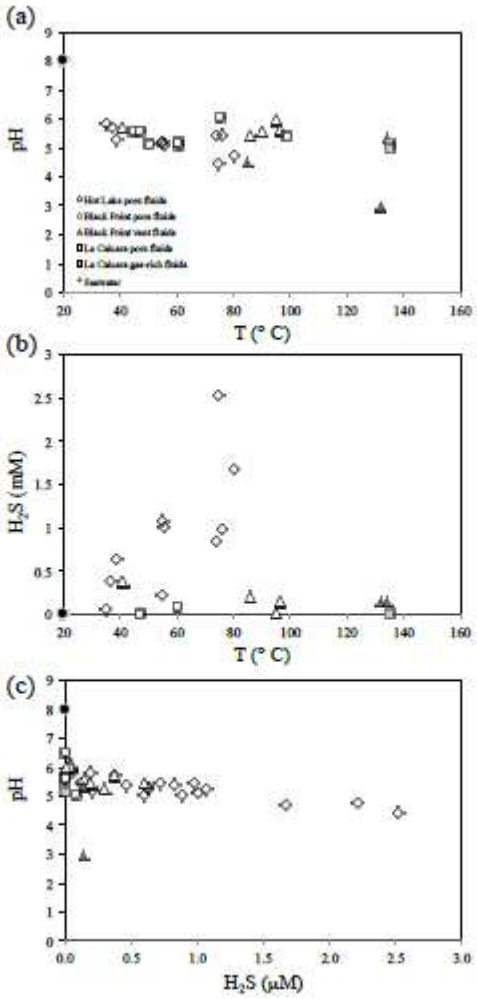

Fig. 4.

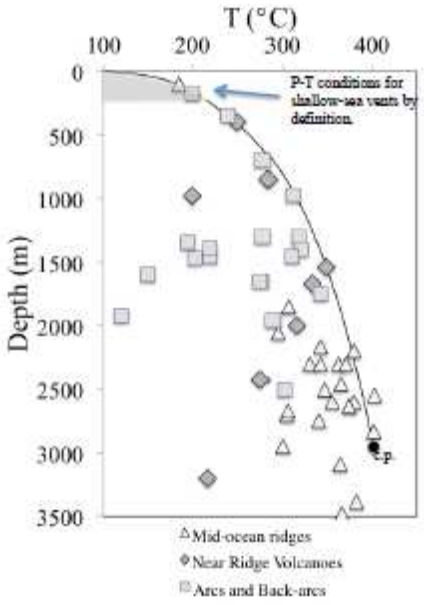

Fig. 5.

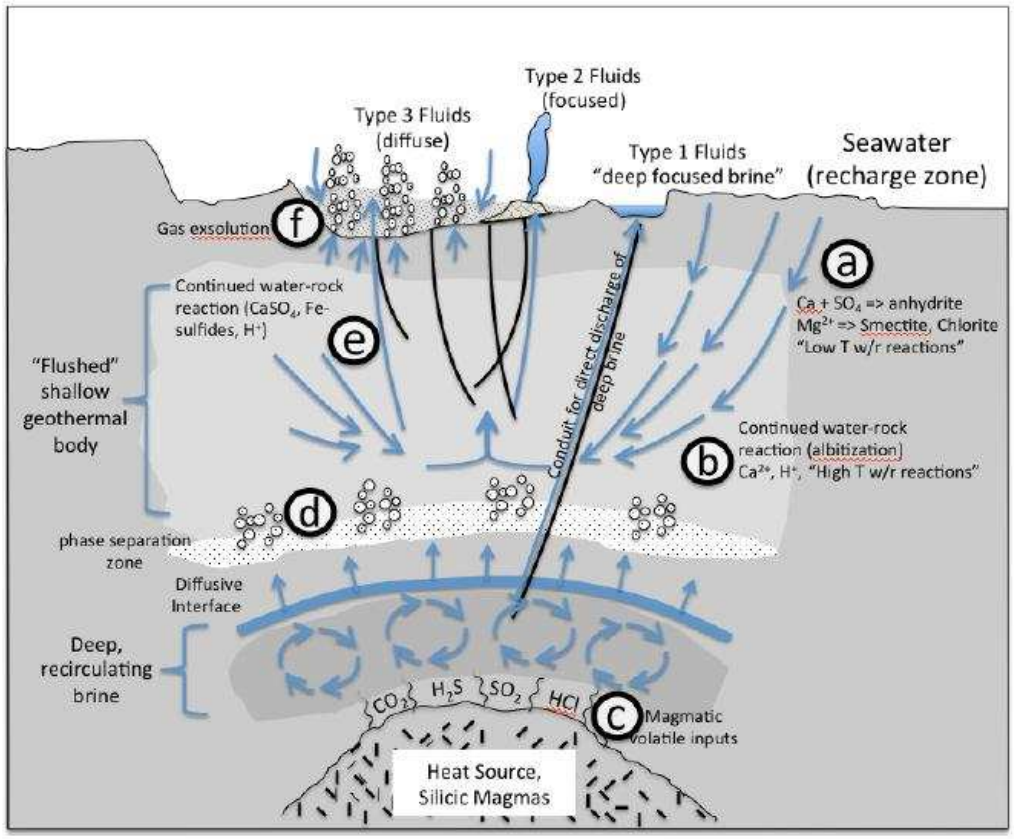

Fig. 6.

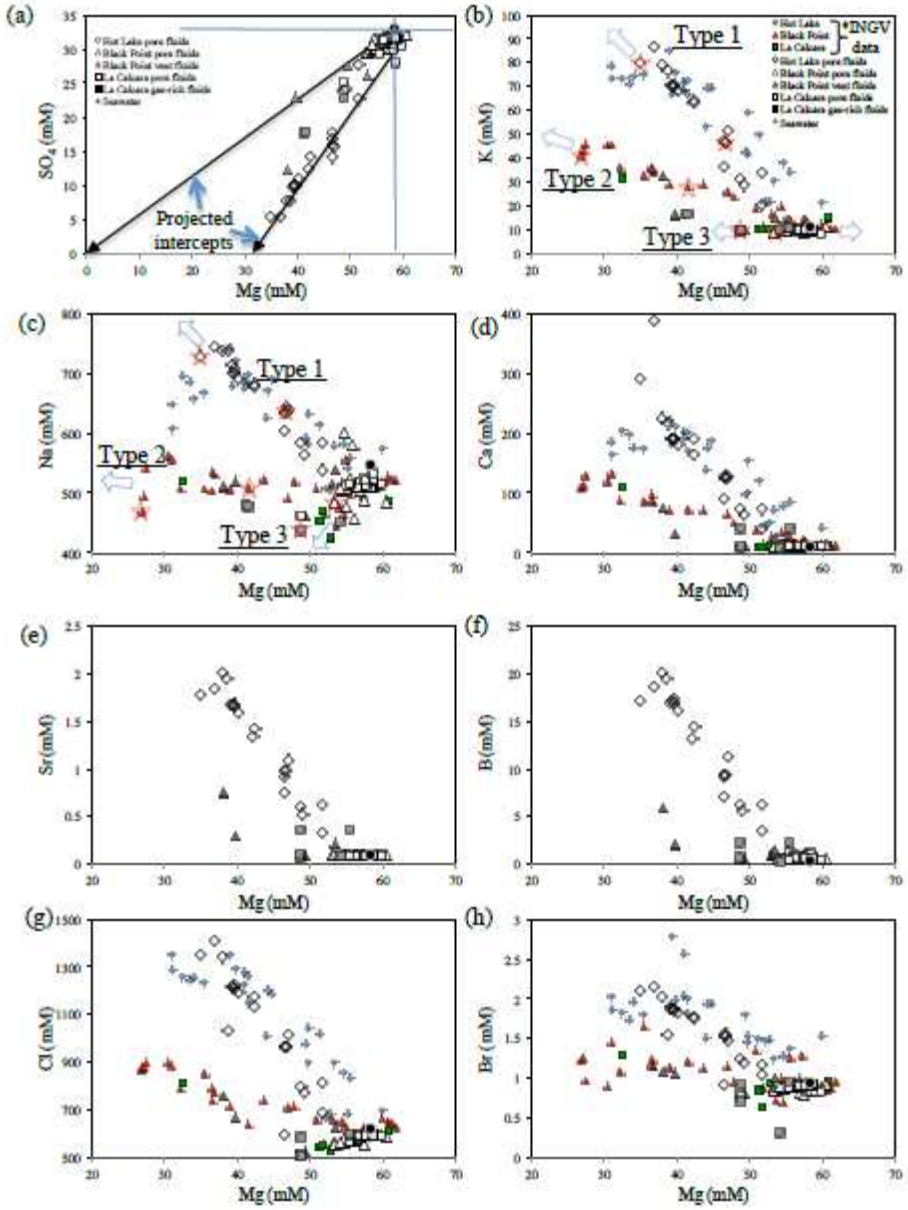

Fig. 7.

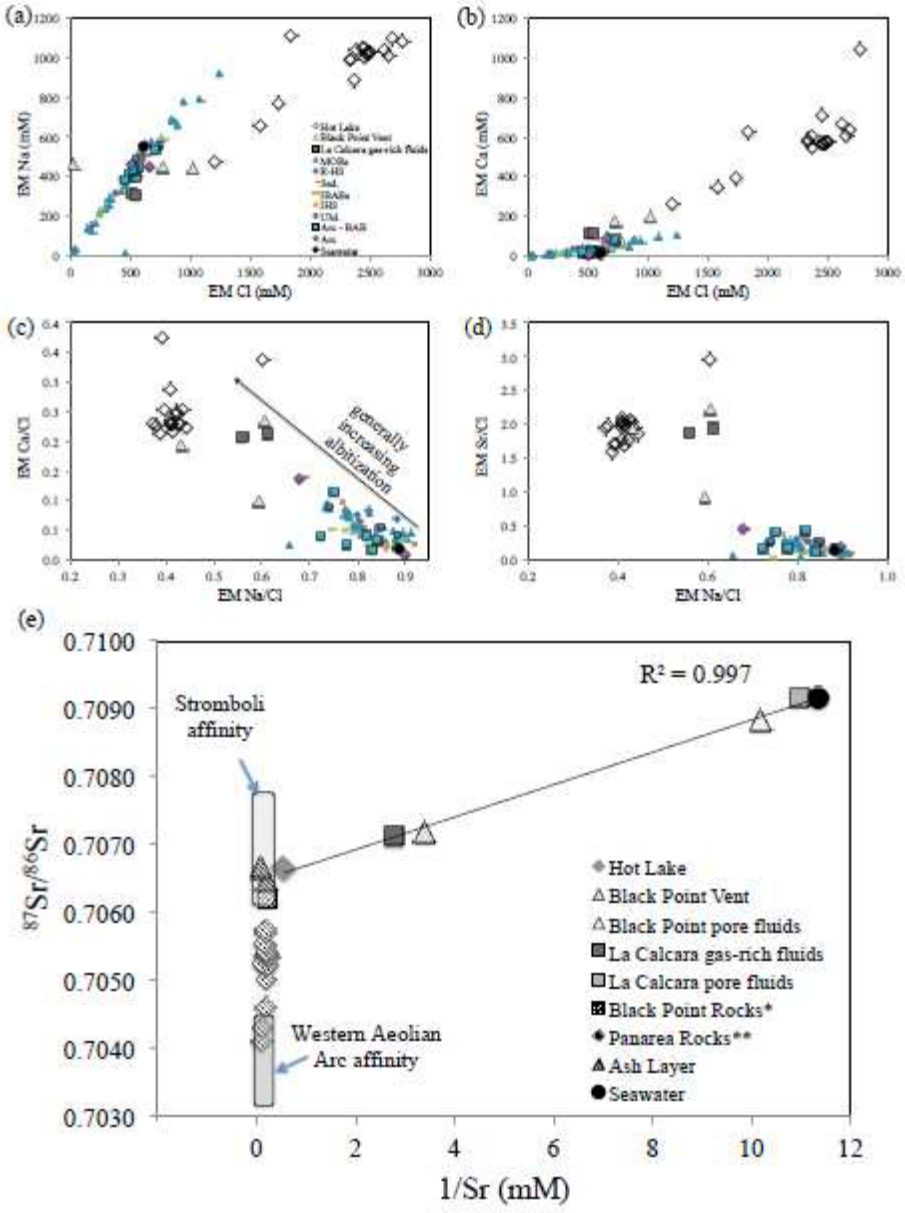

Fig. 8.

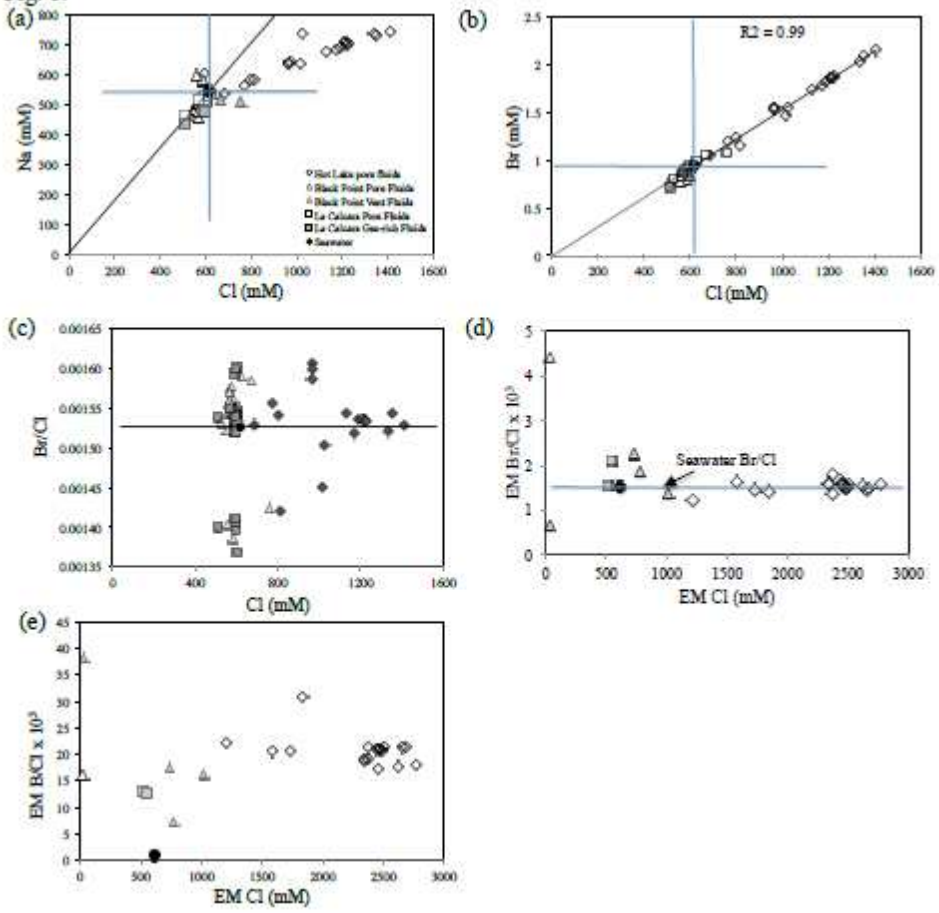

Fig. 9. (a)

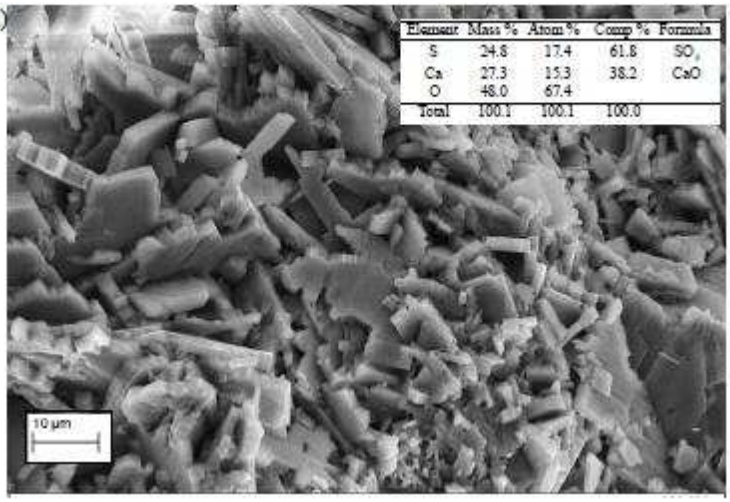

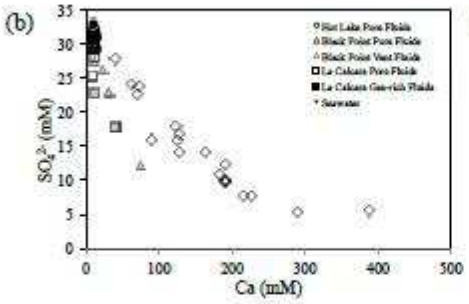

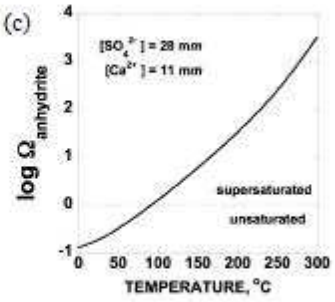

Fig. 10.

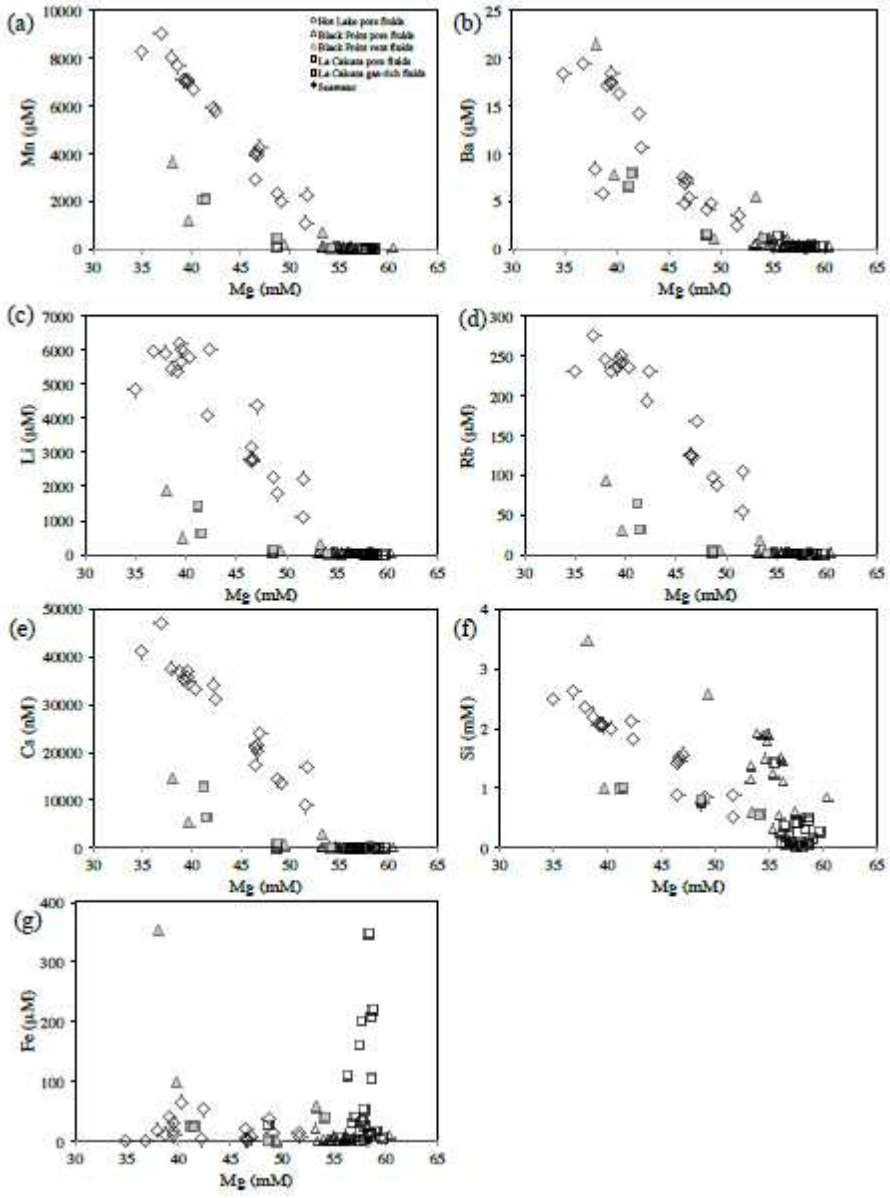

Fig. 11.

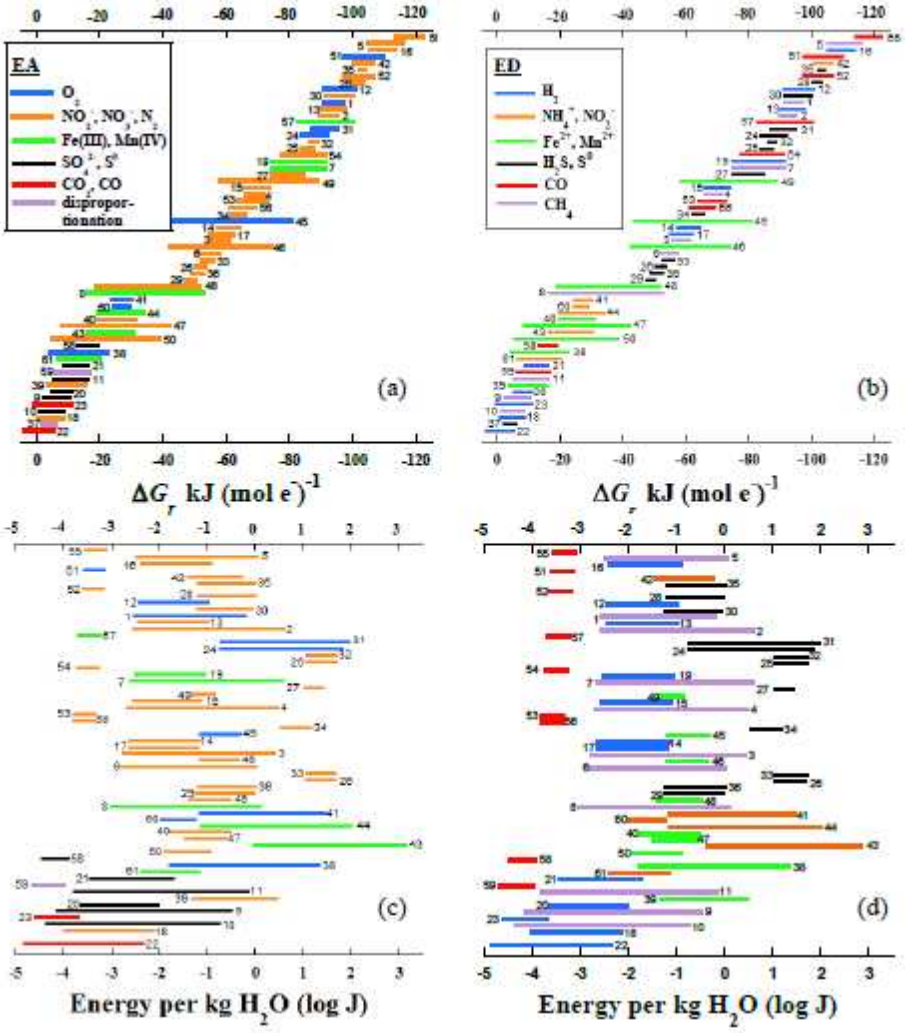

Fig. 12.

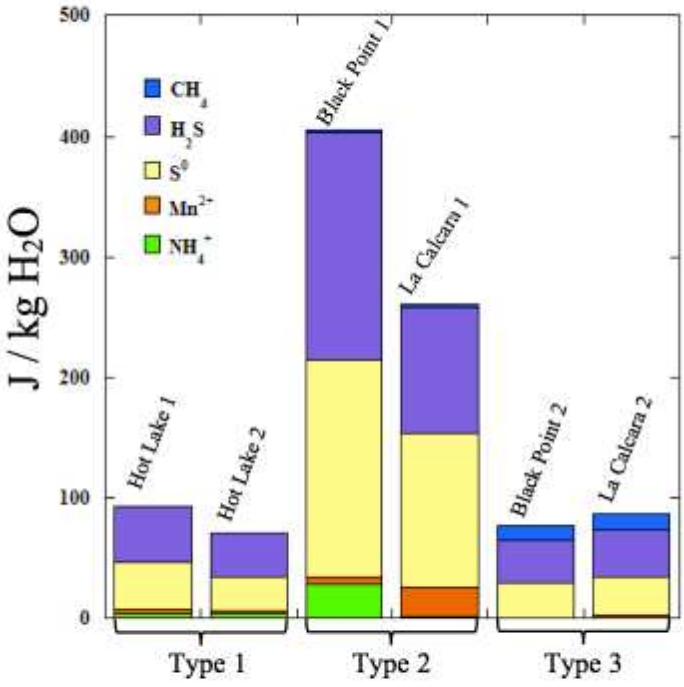

Table 1
Major physicochemical parameters, major and minor elements in hydrothermal fluids from three shallow-sea vents offshore Panarea.

Site	Year	Sample Type[a]	Depth (cm)	Temp °C	pH	H_2S mM	Mg mM	SO_4 mM	Na mM	Ca mM	K mM	B mM	Sr mM	Br mM	Cl mM	Si mM	Fe (total) µM[a]	Mn (total) µM[a]	Ba µM	Li µM	Rb µM	Cs nM	$^{87}Sr/^{86}Sr$
		Seawater	-	~20	8.0	0	58.3	32.9	547	11.1	11.0	0.46	0.09	0.94	618	0.04	0.017	0.0055	0.03	35.1	1.7	2.0	0.709160
Site Lisky	2008	RPF	10				51.7	22.5	585	71.8	33.7	6.1	0.62	1.2	816	0.9	7.1	2270	3.6	2219	104	16790	
	2008	RPF	25				47.0	15.7	637	126.0	51.7	11.3	1.09	1.5	1010	1.6	5.7	4280	5.3	4363	167	24100	
	2009	RPF-1	2	35	5.5	0.05	51.6	27.8	538	39.7	20.3	3.5	0.33	1.0	686	0.5	11.8	1100	2.6	1098	54	8773	
	2009	RPF-1	6		5.8	0.20	48.8	23.8	584	72.5	31.0	6.2	0.60	1.2	800	0.7	37.6	2320	4.1	2267	97	14260	
	2009	RPF-1	10	37	5.7	0.38	46.5	16.0	603	90.5	36.4	7.1	0.76	0.9	594	0.9	18.7	2930	4.7	3110	123	17290	
	2009	RPF-1	14		5.4	0.47	42.4	14.1	677	165.0	63.8	14.4	1.42	1.7	1130	1.8	52.9	5780	10.6	6014	231	31990	
	2009	RPF-1	18		5.0	0.59	38.0	7.7	740	227.0	79.2	20.2	2.00	2.0	1340	2.4	17.2	8050	8.4	5920	266	37570	
	2009	RPF-1	21	39	5.3	0.63	38.7	7.6	737	217.0	76.3	19.4	1.94	1.5	1030	2.2	10.6	7650	5.8	5439	231	36800	
	2009	RPF-2	2		5.5	0.12	49.1	24.1	564	63.5	28.3	5.5	0.53	1.2	770	0.8	13.3	1990	4.7	1772	87	13460	
	2009	RPF-2	6		5.3	0.63	40.3	10.9	693	183.0	67.9	16.2	1.59	1.8	1190	2.0	64.2	6690	16.3	5779	235	33300	
	2009	RPF-2	10	74	5.4	0.83	39.2	9.8	713	192.0	70.5	17.0	1.67	1.9	1220	2.1	39.7	7070	17.1	5377	234	35290	
	2009	RPF-2	14		5.4	0.72	39.5	9.7	700	192.0	70.0	17.2	1.67	1.9	1220	2.1	28.0	7050	17.2	6182	244	34980	
	2009	RPF-2	18	76	5.4	0.98	39.5	10.0	709	190.0	70.0	16.9	1.66	1.9	1210	2.1	17.0	6980	17.5	5679	240	35790	
	2009	RPF-2	22		5.0	0.88	39.6	10.0	703	192.0	70.9	17.6	1.68	1.9	1230	2.0	8.5	7060	18.4	6008	249	36840	
	2010	RPF-1	10	55	5.2	0.22	46.7	14.0	645	129.0	46.8	9.4	0.98	1.6	968	1.4	1.9	4040	7.2	2792	122	20120	
	2010	RPF-1	15	55	5.2	1.07	46.5	16.7	636	128.0	47.0	9.4	0.97	1.5	967	1.4	1.8	4020	7.5	2816	125	20880	
	2010	RPF-1	20	56	5.1	1.00	46.6	17.8	636	124.0	46.3	9.2	0.92	1.5	963	1.5	0.9	3910	6.9	2730	124	21270	
	2010	SPF	10	80	4.7	1.67	35.0	5.4	729	290.0	79.8	17.1	1.78	2.1	1350	2.5	0.4	8250	18.3	4823	231	42980	0.706642
	2010	SPF	10	75	4.4	2.52	36.9	5.5	745	390.0	86.7	18.7	1.84	2.2	1410	2.6	0.4	9050	19.4	5957	275	47090	
	2010	SPF	10		4.8	2.21	42.2	12.4	683	192.0	63.2	13.2	1.33	1.8	1170	2.1	2.8	5800	14.2	4095	193	34870	
Site Palm	2008	RPF	9				57.0	30.0	505	10.7	10.2	0.5	0.10	0.8	583	0.1	7.2		0.5	31	2	64	
	2008	RPF	14				57.5	30.1	487	11.7	8.8	0.5	0.10	0.8	558	0.6	1.0		0.5	32	1	65	
	2008	VF	-	132	2.9	0.15	38.1	12.3	511	78.5	32.6	6.0	0.75	1.1	758	3.5	356	3650	21.5	1883	93	14560	
	2009	RPF	2		6.1	b.d.	55.4	31.2	512	10.5	10.2	1.3	0.09	0.9	589	0.3	b.d.		0.2	28	2	18	
	2009	RPF	6		6.0	b.d.	56.0	31.3	514	10.7	10.2	1.2	0.09	0.9	593	0.3	b.d.		0.2	42	2	14	
	2009	RPF	10	95	6.0	b.d.	56.7	31.1	516	10.8	10.2	1.1	0.09	0.9	589	0.2	3.9		0.3	39	2	12	
	2009	RPF	14		5.6	0.05	53.2	29.4	487	10.9	8.9	1.1	0.09	0.9	563	1.1	21.2	76	0.5	67	2	107	
	2009	RPF	18	97	5.6	0.05	53.4	29.3	483	11.1	8.8	1.1	0.09	0.8	555	1.4	10.0	91	0.5	73	2	112	
	2009	VF	-	134	5.3	0.15	49.4	27.5	462	11.1	10.2	0.6	0.09	0.8	529	2.6	0.5	161	1.1	134	5	588	
	2010	RPF-1	4			0.02	56.0	31.0	580	11.6	10.7	0.5	0.10	0.9	586	0.5	1.0	51	0.3	43	2	127	
	2010	RPF-1	6				54.4	29.6	503	12.9	9.8	0.5	0.10	0.9	566	1.9	0.8	138	0.4	64	3	133	
	2010	RPF-1	8			0.15	55.4	30.5	522	12.1	10.4	0.5	0.10	0.9	581	1.2	1.4	83	0.4	54	3	140	
	2010	RPF-1	12			0.16	54.8	30.0	508	12.9	10.2	0.5	0.10	0.9	568	1.8	0.8	131	0.4	59	3	165	
	2010	RPF-1	20			0.03	54.7	29.9	502	13.0	9.6	0.5	0.10	0.9	561	1.9	0.2	138	0.4	64	3	126	
	2010	RPF-2	2	61	5.7	0.11	60.4	32.1	485	13.1	11.3	0.5	0.11	0.9	590	0.9	10.0	62	0.3	45	2	86	
	2010	RPF-2	6		5.5	0.39	56.1	31.4	458	13.0	10.2	0.5	0.10	0.9	570	1.5	5.2	79	0.4	55	2	123	
	2010	RPF-2	10	88	5.4	0.33	56.3	31.8	512	12.5	10.3	0.5	0.10	0.9	580	1.1	0.9	60	1.1	49	2	125	
	2010	RPF-2	14		5.5	0.37	56.2	31.5	517	12.9	10.2	0.5	0.10	0.9	577	1.4	10.6	82	1.0	55	3	148	
	2010	RPF-2	18	90	5.6	0.30	55.0	31.3	479	13.2	9.9	0.5	0.10	0.9	568	1.9	7.9	112	1.1	62	3	134	
	2010	SPF	10			0.20	54.7	31.4	514	12.0	11.0	0.5	0.10	0.9	576	1.5	1.4	79	1.2	58	3	239	
	2010	SPF	10			0.61	54.0	30.6	507	11.7	10.9	0.5	0.10	0.9	566	1.9	2.4	70	1.3	61	3	220	0.708836
	2010	VF	-	85	4.5		39.7	22.9	520	32.0	16.4	2.1	0.29	1.1	670	1.0	98.7	1178	7.8	693	30	5280	0.707190
	2010	VF	-				53.4	26.2	538	24.6	15.4	1.5	0.22	1.0	628	0.6	56.8	682	5.6	286	18	2848	
Site Cekyan	2008	RPF	3				58.0	30.0	518	10.8	11.0	0.7	0.10	0.8	596	0.0			0.2	45	2	64	
	2008	RPF	15				58.5	28.0	513	10.8	10.0	0.5	0.10	0.8	596	0.1	10.8		0.2	23	1	62	
	2008	RPF	25				59.1	31.2	515	11.0	9.0	0.5	0.10	0.8	602	0.2	16.1		0.2	10	1	62	
	2008	RPF	35				59.7	30.5	515	11.0	8.5	0.5	0.10	0.8	593	0.3	4.5		0.3	8	1	62	
	2008	GRF	-				48.7	22.9	458	10.5	10.3	0.7	0.10	0.7	511	0.8	0.8	427	1.5	126	5	772	
	2009	RPF-1	2		5.5		57.1	31.8	511	10.9	9.8	0.8	0.09	0.9	597	0.1	39.8		0.2	36	2	28	
	2009	RPF-1	6		5.6		57.9	32.1	518	11.1	9.5	0.5	0.09	0.9	606	0.0	52.0		0.1	32	1	12	
	2009	RPF-1	10	44	5.6		57.6	31.4	509	11.1	9.4	0.6	0.09	0.9	594	0.0	15.8		0.1	33	1	6	
	2009	RPF-1	14		5.6		58.3	31.6	522	11.3	9.4	0.4	0.10	0.9	598		11.4		0.2	29	1	3	
	2009	RPF-1	18		5.5	0.001	58.0	30.9	512	11.4	9.5	0.9	0.10	0.9	593	0.1	23.8		0.2	30	1	4	
	2009	RPF-1	21	47	5.6	0.001	57.7	31.4	513	11.5	9.5	0.6	0.10	0.9	602	0.0	32.6	1	0.2	29	1	3	
	2009	RPF-2	2		6.5		56.2	30.9	515	10.7	10.6	0.8	0.09	0.9	585	0.1			0.2	42	2	5	
	2009	RPF-2	6		6.5		56.6	31.0	513	10.8	10.5	0.8	0.09	0.9	590	0.1	2.1		0.2	42	2	5	
	2009	RPF-2	10	75	6.1		57.9	31.6	515	11.1	10.6	1.0	0.10	0.9	595	0.1	0.9		0.2	41	2	5	
	2009	RPF-2	14		5.8	0.001	58.7	31.3	512	11.3	10.2	0.9	0.10	0.9	593	0.1	12.0		0.2	42	2	6	
	2009	RPF-2	18	99	5.6		58.3	31.4	509	11.1	9.6	1.2	0.09	0.9	592	0.3	347		0.2	35	1	4	
	2009	RPF-2	22		5.6		58.5	31.7	509	11.2	9.0	0.5	0.09	0.9	596	0.1	207	1	0.2	18	1	3	
	2009	RPF-3	2		5.5		56.8	31.4	519	10.8	10.2	0.4	0.09	0.9	591	0.2	29.5		0.3	36	2	6	
	2009	RPF-3	6		5.2		58.7	31.7	521	11.1	10.2	0.6	0.09	0.9	598	0.5	220		0.3	37	2	6	
	2009	RPF-3	10	50	5.1		57.7	31.8	512	11.0	9.9	0.5	0.09	0.9	598	0.4	201		0.3	39	2	4	
	2009	RPF-3	14		5.1		57.5	31.6	526	10.9	9.7	0.7	0.09	0.9	593	0.4	160	1	0.3	35	1	6	
	2009	RPF-3	18		5.0		56.4	31.4	510	10.7	9.4	0.6	0.09	0.9	593	0.4	109		0.3	37	1	5	
	2009	RPF-3	22	61	5.1		58.6	31.5	534	11.2	9.8	0.7	0.09	0.9	594	0.5	105		0.4	34	1	5	
	2009	GRF	-	135	5.2	0.01	54.2		452	9.6	9.9	0.3	0.09	0.3		0.6	38.4	19	1.1	30	2	12	0.709208
	2010	SPF	10				48.7	25.2	462	9.1	9.7	0.5	0.08	0.8	510	0.8	26.4	62	1.5	36	2	37	
	2010	SPF	10	60	5.2	0.09	55.5	29.3	516	10.9	10.8	0.5	0.09	0.9	569	1.4	6.6	7	1.4	47	2	118	0.709157
	2010	GRF	-				41.2	17.7	480	40.2	16.6	2.3	0.36	0.9	589	1.0	24.3	2090	6.5	1414	64	12780	0.707119
	2010	GRF	-	135	5.0		41.5	17.8	478	40.6	16.8	2.3	0.36	1.0	597	1.0	24.3	2110	8.0	818	31	6468	

* n.a. = not analyzed
** b.d. = below detection
[a] SPF = Syringe pore fluids; RPF = Rhizon pore fluids (added number differentiates between multiple cores collected in the same year); VF = vent fluids; and GRF = gas-rich fluids
[b] Seawater Fe concentrations from Achterberg et al., 2001. Seawater Mn concentration from Lan and Alfaui, 1994.

Table 2.
End-member concentrations based on zero-Mg, and selected element ratios, for Panama hydrothermal sites investigated in this study compared to other settings.

Site	Year	Sample Type	SO_4	Na	Ca	K	B	Sr	Br	Cl	Si	Ba	Li	Rb	Cs	Na/Cl	Ca/Cl	K/Cl	B/Cl	Br/Cl	Br/Cl	Sr/Ca
			mM	mM	mM	mM	mM	mM	mM	mM	mM	µM	µM	µM	nM				$x10^3$	$x10^3$	$x10^3$	$x10^3$
Star Lake	2008	RFF	**	883	547	212	50.3	46	3.2	2373	7.4	31.6	19330	902	148300							
	2008	RFF		1013	605	221	56.4	5.3	3.8	2663	7.9	37.2	22370	856	124300	0.38	0.23	0.08	21.2	1.99	1.44	8.8
	2009	RFF-1		471	260	93	26.9	1.9	1.5	1214	4.0	22.4	9286	454	76320	0.39	0.21	0.08	22.2	1.58	1.20	7.4
	2009	RFF-1		772	388	134	35.7	3.2	2.5	1739	4.3	25.0	13730	584	87490	0.44	0.22	0.08	20.5	1.65	1.46	8.3
	2009	RFF-1		824	403	136	33.3	3.6	0.7		4.2	23.1	15230	603	85390							8.9
	2009	RFF-1		1026	575	205	51.6	4.9	3.7	2497	6.5	38.8	21960	861	114000	0.41	0.23	0.08	20.7	1.96	1.49	8.5
	2009	RFF-1		1101	630	207	57.2	5.6	4.0	2684	6.7	34.1	16940	698	107900	0.41	0.23	0.08	21.3	2.08	1.48	8.8
	2009	RFF-1		1113	623	205	56.8	5.5	2.6	1843	6.5	37.2	16110	682	109400	0.60	0.34	0.11	30.8	2.97	1.41	8.8
	2009	RFF-2		656	343	121	32.4	2.7	2.0	1502	5.2	29.6	11040	542	85240	0.41	0.22	0.08	20.5	1.70	1.64	7.8
	2009	RFF-2		1020	568	195	51.4	5.0	3.7	2479	6.4	52.7	18640	757	107800	0.41	0.23	0.08	20.7	2.01	1.50	8.8
	2009	RFF-2		1054	564	193	50.9	5.0	3.9	2449	6.2	52.1	16360	712	107700	0.43	0.23	0.08	20.8	2.04	1.58	8.9
	2009	RFF-2		1023	572	194	52.4	5.1	3.9	2484	6.3	53.3	19100	753	108500	0.41	0.23	0.08	21.1	2.05	1.58	8.9
	2009	RFF-2		1049	566	194	51.4	5.1	3.9	2458	6.3	54.2	17540	748	113000	0.43	0.23	0.08	20.9	2.07	1.59	9.0
	2009	RFF-2		1033	575	198	53.3	5.1	3.9	2510	6.3	57.3	18660	774	114000	0.41	0.23	0.08	21.2	2.04	1.57	8.9
	2010	RFF-1		1041	602	191	45.4	4.7	4.3	2580	7.1	36.1	13890	604	101100	0.44	0.25	0.08	19.1	1.96	1.79	7.7
	2010	RFF-1		989	587	189	44.6	4.6	3.7	2542	6.8	36.9	13770	613	103100	0.42	0.25	0.08	19.1	1.96	1.58	7.8
	2010	RFF-1		991	575	186	44.0	4.1	3.7	2539	7.4	34.3	13460	610	106000	0.42	0.25	0.08	18.8	1.76	1.68	7.2
	2010	SFF		1064	709	193	42.1	4.4	3.8	2457	6.2	45.7	12010	574	102500	0.43	0.29	0.07	17.1	1.73	1.56	6.2
	2010	SFF		1086	1042	217	50.2	4.7	4.4	2576	7.0	52.8	16170	747	123500	0.39	0.38	0.08	18.1	1.71	1.58	4.6
	2010	SFF		1039	665	200	46.6	4.5	4.1	2626	7.6	51.3	14780	696	123300	0.40	0.25	0.08	17.7	1.70	1.54	6.7
Black Point	2008	RFF					2.3	0.5			4.1	31.1			2787							
	2008	RFF			55		3.4	0.8			41.6	34.3			4615							14.9
	2008	VF		444	197	73	16.4	2.0	1.6	1024	10.0	62.0	5370	264	40030	0.43	0.19	0.07	16.1	1.95	1.37	10.1
	2009	RFF					17.3	0.1	0.1	31	5.5	3.4		4	310				565.4	2.93	6.43	
	2009	RFF			1		19.2	0.1			5.6	4.3	210	4	306							93.7
	2009	RFF					23.8	0.1			5.5	9.9	170	3	348							
	2009	RFF			9		7.9	0.1	0.5		12.7	5.4	403	6	1203							10.2
	2009	RFF			11		8.1	0.1			12.7	5.6	457	8	1308							8.1
	2009	VF			11	6	1.4	0.1		36	16.6	7.0	692	23	3837		0.31	0.16	38.2	2.58		8.1
	2010	RFF-1			24	3	1.5	0.3			13.0	6.9	230	19	3183							14.4
	2010	RFF-1			38		1.1	0.2	0.3		27.7	5.6	467	17	1963							6.3
	2010	RFF-1		52	31		1.3	0.3	0.1		24.2	7.5	607	20	2955							9.3
	2010	RFF-1			41		1.1	0.3	0.3		29.0	6.2	427	22	2710							6.2
	2010	RFF-1			42		1.1	0.3	0.3		30.5	6.0	500	16	1978							6.0
	2010	RFF-2			1177	330	23.8	11.8			472.0	157.0	5690	235	48860							10.0
	2010	RFF-2			61		1.5	0.4			39.0	9.8	562	20	3201							5.8
	2010	RFF-2	0.8		52		1.6	0.4			31.5	31.2	646	19	3582							7.3
	2010	RFF-2			61		1.6	0.4			38.9	37.0	599	24	4069							6.0
	2010	RFF-2	4.6		48		1.3	0.3	0.2		32.9	18.9	509	16	2327							5.5
	2010	SFF	8.6	16	26	11	1.1	0.3	0.3		23.7	19.0	406	23	3834							9.8
	2010	SFF	1.7	1	19	16	1.0	0.2	0.4		25.4	17.2	382	18	2964							11.7
	2010	VF	1.6	464	77	28	5.6	0.7	1.4	780	3.0	24.4	1471	81	16570	0.58	0.10	0.04	7.2	0.92	1.85	9.4
	2010	VF		447	172	63	12.9	1.6	1.7	735	6.6	66.3	3018	191	33860	0.61	0.23	0.09	17.4	2.23	2.25	9.5
La Gloria	2008	RFF				11	47.1	2.0				33.1	1990	21	12130							
	2008	RFF					23.8	5.9			11.7	99.1			35160							
	2008	RFF					23.8	5.9			70.0	99.1			34810							
	2008	RFF					23.8	5.9			134.0	157.0			34691							
	2008	GRF			7	7	1.9	0.2			4.7	9.0	589	21	4681							20.2
	2009	RFF-1			1		17.0	0.1			3.0	8.3	84		1270							65.1
	2009	RFF-1			11		6.3	0.1				10.2			1430							8.1
	2009	RFF-1			11		12.1	0.1				5.9			302							8.1
	2009	RFF-1			128			5.9				99.1			700							46.4
	2009	RFF-1			69		86.0	2.0			3.9	33.1			294							29.3
	2009	RFF-1			50		14.1	1.1			0.0	16.5			138							21.2
	2009	RFF-2					9.9	0.1			1.4	4.7	232	7	86							
	2009	RFF-2			1		12.1	0.1			0.4	5.9	275	5	95							110.9
	2009	RFF-2			11		79.2	1.5			10.2	24.8	910	16	381							139.4
	2009	RFF-2			128		257.0	5.9			35.0	99.1	4291		993							46.4
	2009	RFF-2			11		402.0	0.1			152.0	99.1	93		1343							8.1
	2009	RFF-2			69		23.8	0.1			23.4	99.1			352							1.3
	2009	RFF-3						0.1			7.0	10.5	58	2	161							
	2009	RFF-3			11		92.1	0.1			245.0	157.0	1201		2509							8.1
	2009	RFF-3			1		4.3	0.1			37.9	26.3	375		206							65.1
	2009	RFF-3					13.0	0.1			27.7	19.7	35		286							
	2009	RFF-3					4.8	0.1			10.2	8.3	84		88							
	2009	RFF-3			69		146.0	0.1			274.0	216.0			1518							1.3
	2009	GRF						0.1			7.3	15.2		0	144							
	2010	SFF		33			3	0.7	0.0	0.1	4.4	9.0	40	2	214							
	2010	SFF			7	7	1.3	0.1	0.1		29.0	28.4	283	10	3424							13.0
	2010	GRF		317	110	36	6.7	1.0	0.8	518	3.3	32.1	4736	213	43560	0.61	0.21	0.06	13.0	1.95	1.55	9.0
	2010	GRF		306	113	31	6.8	1.0	1.1	547	3.4	37.7	2056	104	22440	0.56	0.21	0.06	12.5	1.88	2.10	9.1
Mid-ocean ridges			0.4	417	35	23		0.1		533	13.1	79.7	668			0.79	0.06	0.04		0.39		3.3
Ridge hot spot intersections			0.4	355	31	21		0.1		451	14.0	29.8	350			0.83	0.07	0.05		0.24		3.5
Ultramafic hosted			4.3	469	39	22		0.2		605	7.5	34.5	290			0.83	0.06	0.03		0.27		3.9
Sedimented ridges			0.2	458	43	33		0.2		581	11.6	36.0	784			0.79	0.08	0.05		0.37		5.4
Intraoceanic back-arc basins			4.6	418	30	34		0.1		534	12.1	34.8	1159			0.80	0.05	0.06		0.18		6.1
Volcanic arcs			16.0	455	47	26		0.2		587	7.4	106.0	314			0.79	0.07	0.03		0.32		13.7
Transitional arc - back-arc basins			5.3	434	27	49		0.2		552	11.3	47.0	2163			0.79	0.05	0.09		0.26		5.7
Intraplate hot spot volcanoes			26.0	427	11	11		0.1		515	1.2		79			0.85	0.02	0.02		0.17		7.2

Note: Representative Major Element Composition of End-Member Fluids from Selected Sea-Floor Hydrothermal Vents from Hannington et al. (2005)
** blank cells calculated to negative values

Table 3
Summary of geochemical parameters used for calculating the theoretical bioenergetics for inferred site and fluid type compositions investigated at Panarea.

Sample/site	Fluid Type	Temp °C	pH	Na^+ mM	K^+ mM	Mg^{2+} mM	Ca^{2+} mM	Cl^- mM	Br^- mM	SO_4^{2-} mM	SiO_2 mM	B^{3+} mM	Sr^{2+} mM	Mn^{2+} mM	Fe^{2+} mM	Ba^{2+} mM
Seawater	n.a.	20	8.02	546.9	11.0	58.3	11.1	617.7	0.9	32.9	0.04	0.46	0.10	5.E-06	1.00E-16*	0.034
Hot Lake 1	1	80.1	4.7	729.5	79.8	35.0	290.1	1352.6	2.1	5.4	2.5	17.1	1.78	6.37[x]	0.0145[x]	0.018
Hot Lake 2	1	54.7	5.2	645.2	46.8	46.7	128.7	968.3	1.6	14.0	1.4	9.4	0.98	6.14[x]	0.009[x]	0.017
Black Point 1	2	135.0	2.9	511.4	32.6	38.1	75.5	758.4	1.1	12.3	3.5	6.0	0.75	4.15[x]	0.19[x]	0.022
Black Point 2	3	96.6	5.6	483.4	8.8	53.4	11.1	554.9	0.8	29.3	1.4	1.1	0.09	1.38[x]	0.035[x]	0.504
La Calcara 2	2	135.0	5.0	477.6	16.8	41.5	40.6	597.4	1.0	17.8	1.0	2.3	0.36	2.1*	0.024*	0.008
La Calcara 1	3	60.3	5.2	515.7	10.8	55.5	10.9	568.5	0.9	29.3	1.4	0.5	0.09	0.007*	0.007*	0.001

		HCO_3^- mM	H_2S mM	O_2 mM	NO_3^- mM	NO_2^- mM	NH_4^+ mM	$CO_{2(g)}$ %	$H_2S_{(g)}$ vol %	$O_{2(g)}$ %	$N_{2(g)}$ %	$CO_{(g)}$ ppm	$CH_{4(g)}$ ppm	$H_{2(g)}$ ppm
Seawater	n.a.	2.3	2 nM	0.24	0.0081	0.0002	0.0005	n.a.	n.a.	n.a.	n.a.	n.a.	n.a.	n.a.
Hot Lake 1	1	1.04[$]	1.67	0.025[x]	0.027[&]	0.0002[$]	3.39[$]	96.4	2.7	0.02	0.5	4.0	5.0	35.0
Hot Lake 2	1	1.48[$]	0.22	0.04[$]	0.027[&]	0.0002[$]	1.69[$]	96.4	2.7	0.02	0.5	4.0	5.0	35.0
Black Point Vent 1	2	0.8[&]	0.15	0.194[x]	0.11[&]	0.0005[$]	1.69[$]	98.7	0.3	0.03	0.4	3.2	817.3	91.3
Black Point Vent 2	3	2.4[$]	0.05	0.24[$]	0.034[&]	0.0005[$]	0.003[$]	98.7	0.3	0.03	0.4	3.2	817.3	91.3
La Calcara 1	2	n.a.[#]	n.a.	n.a.	0.027[&]	0.0003	0.18[&]	97.2	0.2	0.08	0.9	3.0	5306.5	694.8
La Calcara 2	3	n.a.	0.086	n.a.	0.027[&]	0.0003	0.18[&]	97.2	0.2	0.08	0.9	3.0	5306.5	694.8

notes: Seawater values for aqueous H_2S from Luther and Tsamakis (1989). Aqueous seawater values for CH_4, H_2, CO, and N_2 are from Charlou et al. (2002). Seawater Mn^{2+} from Klinknhammer et al. (1985). NO_3^- values at Hot lake and La Calcara is an average of values from Tassi et al. (2009). Because dissolved O_2 at La Calcara was not reported the equilibrium value for O_2 free gas concentrations were used. NO_2^- at La Calcara is an average of the other sites. #n.a. = not available.
* = equilibrium value calculated using Geochemist's workbench.
$ = from Sieland, 2009 sample with matching Mg concentration.
x = these data points and all dissolved gas data from Müller, 2011.
& = from Tassi et al., 2009

Table 4.

Summary of metabolic reactions consider in the present study

	CH_4 oxidation	32	$5S^0 + 6NO_3^- + 2H_2O \rightarrow 5SO_4^{2-} + 3N_2 + 4H^+$
1	$CH_4 + 2O_2 \rightarrow CO_2 + 2H_2O$	33	$4S^0 + 3NO_3^- + 7H_2O \rightarrow 4SO_4^{2-} + 3NH_4^+ + 2H^+$
2	$5CH_4 + 8NO_3^- + 8H^+ \rightarrow 5CO_2 + 4N_2 + 14H_2O$	34	$S^0 + 3NO_3^- + H_2O \rightarrow SO_4^{2-} + 3NO_2^- + 2H^+$
3	$CH_4 + NO_3^- + 2H^+ \rightarrow CO_2 + NH_4^+ + H_2O$	35	$S^0 + 2NO_2^- \rightarrow SO_4^{2-} + N_2$
4	$CH_4 + 4NO_3^- \rightarrow CO_2 + 4NO_2^- + 2H_2O$	36	$S^0 + NO_2^- + 2H_2O \rightarrow SO_4^{2-} + NH_4^+$
5	$3CH_4 + 8NO_2^- + 8H^+ \rightarrow 3CO_2 + 4N_2 + 10H_2O$	37	$4S^0 + 4H_2O \rightarrow SO_4^{2-} + 3H_2S + 2H^+$
6	$3CH_4 + 4NO_2^- + 8H^+ \rightarrow 3CO_2 + 4NH_4^+ + 2H_2O$		**Mn^{2+} oxidation**
7	$CH_4 + 4MnO_2 + 8H^+ \rightarrow CO_2 + 4Mn^{2+} + 6H_2O$	38	$2Mn^{2+} + O_2 + 2H_2O \rightarrow 2MnO_2 + 4H^+$
8	$CH_4 + 8FeOOH + 16H^+ \rightarrow CO_2 + 8Fe^{2+} + 14H_2O$	39	$5Mn^{2+} + 2NO_3^- + 4H_2O \rightarrow 5MnO_2 + N_2 + 8H^+$
9	$CH_4 + SO_4^{2-} + 2H^+ \rightarrow CO_2 + H_2S + 2H_2O$	40	$3Mn^{2+} + 2NO_2^- + 2H_2O \rightarrow 3MnO_2 + N_2 + 4H^+$
10	$3CH_4 + 4SO_4^{2-} + 8H^+ \rightarrow 3CO_2 + 4S^0 + 10H_2O$		**NH_4^+ oxidation**
11	$CH_4 + 4S^0 + 2H_2O \rightarrow CO_2 + 4H_2S$	41	$NH_4^+ + 1.5O_2 \rightarrow NO_2^- + H_2O + 2H^+$
	H_2 oxidation	42	$NH_4^+ + NO_2^- \rightarrow N_2 + 2H_2O$
12	$H_2 + 1/2O_2 \rightarrow H_2O$	43	$NH_4^+ + 4MnO_2 + 6H^+ \rightarrow NO_3^- + 4Mn^{2+} + 5H_2O$
13	$5H_2 + 2NO_3^- + 2H^+ \rightarrow N_2 + 6H_2O$	44	$NH_4^+ + 3MnO_2 + 4H^+ \rightarrow NO_2^- + 3Mn^{2+} + 4H_2O$
14	$4H_2 + NO_3^- + 2H^+ \rightarrow NH_4^+ + 3H_2O$		**Fe^{2+} oxidation**
15	$H_2 + NO_3^- \rightarrow NO_2^- + H_2O$	45	$4Fe^{2+} + O_2 + 6H_2O \rightarrow 4FeOOH + 8H^+$
16	$3H_2 + 2NO_2^- + 2H^+ \rightarrow N_2 + 4H_2O$	46	$5Fe^{2+} + NO_3^- + 7H_2O \rightarrow 5FeOOH + 0.5N_2 + 9H^+$
17	$3H_2 + NO_2^- + 2H^+ \rightarrow NH_4^+ + 2H_2O$	47	$8Fe^{2+} + NO_3^- + 13H_2O \rightarrow 8FeOOH + NH_4^+ + 14H^+$
18	$3H_2 + N_2 + 2H^+ \rightarrow 2NH_4^+$	48	$2Fe^{2+} + NO_3^- + 3H_2O \rightarrow 2FeOOH + NO_2^- + 4H^+$
19	$H_2 + MnO_2 + 2H^+ \rightarrow Mn^{2+} + 2H_2O$	49	$3Fe^{2+} + NO_2^- + 4H_2O \rightarrow 3FeOOH + 0.5N_2 + 5H^+$
20	$4H_2 + SO_4^{2-} + 2H^+ \rightarrow H_2S + 4H_2O$	50	$6Fe^{2+} + NO_2^- + 10H_2O \rightarrow 6FeOOH + NH_4^+ + 10H^+$
21	$H_2 + S^0 \rightarrow H_2S$		**CO oxidation/disproportionation**
22	$4H_2 + CO_2 \rightarrow CH_4 + 2H_2O$	51	$2CO + O_2 \rightarrow 2CO_2$
23	$3H_2 + CO \rightarrow CH_4 + H_2O$	52	$5CO + 2NO_3^- + 2H^+ \rightarrow 5CO_2 + N_2 + H_2O$
	H_2S oxidation	53	$4CO + NO_3^- + H_2O + 2H^+ \rightarrow 4CO_2 + NH_4^+$
24	$H_2S + 2O_2 \rightarrow SO_4^{2-} + 2H^+$	54	$CO + NO_3^- \rightarrow CO_2 + NO_2^-$
25	$5H_2S + 8NO_3^- \rightarrow 5SO_4^{2-} + 4N_2 + 2H^+ + 4H_2O$	55	$3CO + 2NO_2^- + 2H^+ \rightarrow 3CO_2 + N_2 + H_2O$
26	$H_2S + NO_3^- + H_2O \rightarrow SO_4^{2-} + NH_4^+$	56	$3CO + NO_2^- + H_2O + 2H^+ \rightarrow 3CO_2 + NH_4^+$
27	$5H_2S + 2NO_3^- + 2H^+ \rightarrow 5S^0 + N_2 + 6H_2O$	57	$CO + MnO_2 + 2H^+ \rightarrow CO_2 + Mn^{2+} + H_2O$
28	$3H_2S + 8NO_2^- + 2H^+ \rightarrow 3SO_4^{2-} + 4N_2 + 4H_2O$	58	$4CO + SO_4^{2-} + 2H^+ \rightarrow 4CO_2 + H_2S$
29	$3H_2S + 4NO_2^- + 4H_2O + 2H^+ \rightarrow 3SO_4^{2-} + 4NH_4^+$	59	$4CO + 2H_2O \rightarrow 3CO_2 + CH_4$
30	$3H_2S + 2NO_2^- + 2H^+ \rightarrow 3S^0 + N_2 + 4H_2O$		**NO_2^- oxidation**
	S^0 oxidation/disproportionation	60	$2NO_2^- + O_2 \rightarrow 2NO_3^-$
31	$S^0 + 1.5O_2 + H_2O \rightarrow SO_4^{2-} + 2H^+$	61	$NO_2^- + MnO_2 + 2H^+ \rightarrow NO_3^- + Mn^{2+} + H_2O$

All species are taken to be aqueous except elemental sulfur (S^0), pyrolusite (MnO_2) and goethite (FeOOH), which are all crystalline phases.

Highlights

- Panarea vent fluids show three distinct compositions related to a two-layered hydrothermal system.
- Type 1 fluids are from a deep, brine reservoir; Type 2 fluids are from a shallow, lower salinity reservoir
- The deeper reservoir records some of the highest end-member Cl concentrations to date.
- Type 3 fluids are primarily seawater influenced by degassing of volatiles and mass transfer from gas to aqueous phase.
- Sulfur oxidation reactions with O_2 are the most exergonic and agree with existing microbiology data.